Therapeutic Potential of CPP (NP1) Mediated siRNA Delivery: Evidence in 3D Spheroids of Colon Cancer Cells (HCT 116)

by

Khalsa Al-Husaini

A thesis
presented to the University of Waterloo
in fulfillment of the
thesis requirement for the degree of
Master of Applied Science
in
Chemical Engineering (Nanotechnology)

Waterloo, Ontario, Canada, 2016
© Khalsa Al-Husaini 2016

AUTHOR'S DECLARATION

I hereby declare that I am the sole author of this thesis. This is a true copy of the thesis, including any required final revisions, as accepted by my examiners. I understand that my thesis may be made electronically available to the public.

Abstract

At the forefront of revolutionizing medicine, gene therapy provides a promise to treat a wide range of diseases by regulating defective genes. RNA interference (RNAi) holds great potential as a therapeutic route due to its high efficiency and specific posttranscriptional gene silencing process, which can be triggered by small interfering RNAs. siRNAs are a class of 21 to 23 nucleotide-long double-stranded RNA molecules that inhibit the expression of a specific gene by the degradation of its complementary messenger RNA (mRNA). Despite its potential value, a number of problems remain as major obstacles to clinical applications of therapeutic siRNAs, related to its large molecule weight, negative charge, hydrophilicity, sensitivity to nuclease degradation and short plasma half-life of less than ten minutes. These unfavorable properties lead to instability of naked siRNA under physiological conditions, rapid clearance from the blood stream, and inability to cross target cell membranes. Therefore, siRNAs as a potential therapeutic agent require an efficient and safe delivery carrier that will facilitate their biological functions. A variety of carriers have been developed to deliver siRNA and maximize its therapeutic effects including viruses, lipids, polymers, dendrimers, peptides, and nanoparticles. Cell penetrating peptides (CPPs) have emerged as a promising candidate due to their rapid and high efficient internalization and low toxicity. CPPs mediate siRNA delivery through endocytic pathways or by directly crossing the targeted cell membrane.

As most of preclinical models were carried out in monolayer cell culture, for *in vitro* testing, it is not physiologically relevant to *in vivo* models, where three-dimensional tissues are the object. On the other hand, development of more biologically relevant

models for early drug screening will result in reduction of animal models required, which tend to be expensive and time consuming. Therefore, various 3D cell culture techniques have been developed to produce multicellular spheroids, mainly for cancer drug discovery. Multicellular spheroids are *in vitro* micro-scale tissue analogs, where cell clusters form by self-assembly. Spheroids with radii of 200 μm and larger will develop three different zones of proliferating cells on the outside, quiescent cells on the inside and a necrotic core due to nutrient and oxygen transport limitations. Spheroids harbor several features that make a more physiological platform for early drug discovery due to the following reason: spheroids of multicellular 3D architecture mimic the *in vivo* microenvironment of tumor and extracellular matrix deposition that are found *in vivo* but absent in monolayer culture; spheroids of *in vivo* solid tumor models develop a necrotic core beside the hypoxia present in many cancers; the tight cell-cell interactions are comparable to those in *in vivo* tissues. Taken together, spheroids provide an improved model for testing *in vitro* siRNA delivery of the current interest, compared to regular monolayer cell culture.

The aim of this study is to develop 3D spheroids of HCT 116 colon cancer cell line using the hanging drop method and evaluated NP1, a novel CPP (STR-H16R8) developed by Dr. Chen's group, to assist siRNA delivery, to silence specific targeted genes for therapeutic purposes. Morphological characterization of 3D spheroids generated in hanging drop plates clearly indicates that HCT 116 cells were able to form compact spheroids within 3 days and start to form three distinct layers of proliferating, dormant and necrotic cells, which closely mimic the features of tumors *in vivo*. Furthermore, H&E stained spheroids showed large cohesive cells with apparent epithelial

phenotype, and large atypical nuclei with occasional prominent nucleoli, which closely mimic the features of tumors *in vivo* but not present in 2D cell monolayer. NP1 demonstrated a high gene knockdown efficiency, both in 2D and 3D cell culture, with higher uptake in 2D compared to 3D. NP1-Bcl-2-siRNA showed a 85% knockdown efficiency in 2D and 53% in 3D cell culture. NP1-VEGF-siRNA induced a 72% and 51% reduction in mRNA level in 2D and 3D cell culture, respectively. At the protein level, NP1-Bcl-2-siRNA complexes exhibited significant inhibition of the Bcl-2 protein compared to non-treated cells in western blot results. 3D spheroids showed apoptosis resistance compared to 2D cells. These results demonstrated that compact MCTS closely mimic the features of tumors *in vivo* in term of simulating important tumor characteristics including hypoxia, formation of ECM and necrotic core, anti-apoptotic features and their resulting therapy resistance. The higher silencing efficiency and apoptosis rate observed in 2D compared to 3D clearly indicate that 2D monolayer cells on plastic plates are not physiologically relevant to tumor microenvironment and overestimate the efficacies of tested drugs. NP1 as a siRNA carrier in both cell culture models, efficiently protect, deliver siRNAs and maintain high silencing efficiency.

Acknowledgements

First and foremost, I would like to express my sincere gratitude to my supervisors Professor Pu Chen and Professor Ali Elkamel for all the encouragement, continuous guidance, valuable advices and unconditional support in difficult times.

Secondly, I would like to thank my reading committee members Prof. Boxin Zhao and Prof. Chandra Mouli R. Madhuranthakam, for their time and valuable comments and advices on my thesis.

I would like to thank Dr. Denise Hileeto and Dr. Lakshman Subbaraman for the scientific expertise, guidance, availability and help to do the histological part of work.

To all the group colleagues, specially Xiaoxia Han, Ran Pan, Wen Xu, Baoling Chen, Kaveh Sarikhani, Lei Zhang, Mohammad Ali Shekholeslam, Weijia Cui and Sheng Lu, I would like to acknowledge all these people by their teachings, valuable technical help, feedback, unspeakable patience, friendship, advice and support.

At the end, I would like to thank my family and my friends for providing unlimited support and enormous encouragement. Without their love, none of my achievements would come true. Most of all, I am grateful to my friend Amal Al-Subaei for always encouraging and helping all the way long.

Dedication

To my dear parents, for their never-ending love and support

Table of Contents

List of Figures

List of Tables

List of Abbreviations

Acronym	Full name
AIDS	Acquired immunodeficiency syndrome
AD	Alzheimer's disease
ALS	Amyotrophic lateral sclerosis
ATCC	American Type Culture Collection
Bcl-2	B-cell lymphoma 2
bPEI	Branched polyethylenimine
BSA	Bovine serum albumin
CCK-8	Cell counting kit-8
CLSM	Confocal laser scanning microscopy
CPP	Cell-penetrating peptide
DAB	3'3' diaminobenzidine
DAPI	4',6-diamidino-2-phenylindole
DC-Chol	3β-[*N*-(*N*′,*N*′-dimethylaminoethane)-carbamoyl]cholesterol
DDAB	Dimethyldioctadecyl-ammonium bromide
DLS	Dynamic light scattering
DMEM	Dulbecco's Modified Eagle Medium
DMRIE-C	1,2-dimyristyloxypropyl-3-dimethyl-hydroxy ethyl ammonium bromide-cholesterol
DNA	Deoxyribonucleic acid
DOPC	1,2-oleoyl-sn-glycero-3-phosphocholine
DOPE	1,2-dioleoyl-sn-glycero-3-phosphoethanolamine
DOTAP	1-oleoyl-2-[6-[(7-nitro-2-1, 3-benzoxadiazol-4-yl) amino]hexanoyl]-3-trimethylammonium propane
DOTMA	N-[1-(2,3-dioleoyloxy) propyl]-N,N,Ntrimethylammonium chloride
dsRNA	Double-stranded RNA
ECM	Extracellular matrix
EDTA	Ethylenediaminetetraacetic acid

ESEM	Environmental scanning electron microscope
EthD-1	Ethidium homodimer
FACS	Fluorescence-activated cell sorting
FBS	Fetal bovine serum
GAPDH	Glyceraldehyde 3-phosphate dehydrogenase
HBcAg	Hepatitis B virus core antigen
HBsAg	Hepatitis B virus surface antigen
HBV	Hepatitis B virus
HD	Huntington's disease
HIF-1α	Hypoxia-inducible factor-1α
HIV	Human immunodeficiency virus
Lipo	Lipofectamine 2000
MCTS	Multicellular tumor spheroids
NC	Negative control
nt	Nucleotides
Opti-MEM	Improved Minimal Essential Medium
PBS	Phosphate-bufferred saline
PCR	Polymerase chain reaction
PCL	Poly caprolactone
PD	Parkinson's disease
PEC	Polyelectrolyte complex
PEG	Poly ethylene glycol
PEI	Poly ethyleneimine
PFA	Paraformaldehyde
PI	Propidium iodide
PLA	Poly-d,l-lactide
PLGA	Poly-D, L-lactide-co-glycolide
PLL	Poly-L-lysine
PPI	Poly propylenimine
RISC	RNA-induced silencing complex
RNAi	RNA interference

RT	Room temperature
RT-PCR	Reverse transcriptase PCR
SEM	Scanning electron microscopy
shRNA	Short hairpin RNA
siRNA	Small interfering RNA
STR	Stearic acid
TLRs	Toll-like receptors
VEGF	Vascular endothelial growth factor
WST-1	Water soluble tetrazolium-1

Chapter 1
Overview

1.1 Research Background

By many biologists, the discovery of RNA interference (RNAi) is considered to be one of the most important and valuable breakthrough of the past decade. RNA interference (RNAi) holds great promise as therapeutic agents due to the high efficiency and specific posttranscriptional gene silencing process. RNAi provides an effective potential to treat wide range of diseases by silencing or inhibition of defective genes, which can be triggered by small interfering RNA[1]. In 2006 the values of this discovery gained its inventors, Andrew Z. Fire and Craig C. Mello, the award of Nobel Prize in Physiology or Medicine.

Small interference RNAs (siRNAs), are class of 21 to 23 nucleotide-long double-stranded RNA molecules that inhibits the expression of a specific gene by the degradation of its complementary messenger RNA (mRNA)[2]. The mechanism of RNAi inhibition of defective genes by interfering the translation of mRNA into protein is briefly reviewed here. In general, long dsRNA is the precursor of siRNA, the long dsRNA cleaved into smaller siRNA molecules 21-23 nt by RNase III like enzyme, Dicer, once introduce to the cells[3]. The newly formed ds-siRNA molecules then bind to a protein complex called RNA-induced silencing complex (RISC). Due to the helicase activity of the protein complex siRNA is unwounded into a sense (passenger) strand and an antisense (guide) strand. Guide strand with RISC will be activated and bind to the complementary target mRNA which will be then cleaved and degraded by enzymatic

activity within RISC (argonaute 2)[4–7]. By that the expression of the specific targeted genes into proteins will be prevented or terminated.

Since the discovery of RNAi, there has been an explosion of interest in using this technology for basic and applied research mainly in gene therapy and development of gene-specific drugs as RNAi has been one of the most promising new approaches for disease therapy. Despite its potential value**,** *in vivo* siRNA silencing target gene expression by systemic delivery has been a very challenging task due to its large moleculer weight, negative charge, hydrophilicity, sensitivity to nuclease degradation and short plasma half-life[8]. These unfavorable properties lead to instability of naked siRNA under physiological conditions, rapid excretion, inability to cross target cell membranes and inefficient intracellular release [9]. Therefore, siRNA as a potential therapeutic agent requires efficient and safe delivery that will retain their biological functions.

A wide range of carriers have been developed to deliver siRNA and maximize its therapeutic effects including viruses[10], lipids[11], polymers[12], dendrimers[13], peptides[14], and nanoparticles[15]. Cell penetrating peptides (CPP), are short cationic or amphipathic sequences of about 5-30 amino acids, have emerged as a promising candidate due to rapid and high efficient internalization and low toxicity. CPP mediates siRNA delivery through endocytic pathways or by directly crossing the targeted cell membrane[16].

As most of preclinical models were carried in monolayer cell culture for *in vitro* testing, it is not physiologically relevant to *in vivo* models. Therefore, developing *in vitro* models more relevant to *in vivo* is required for drug discovery. Moreover, development of more biologically relevant models for early drug screening will result in reduction of animal models required and improves the success rate. Various 3D cell culture techniques

have been developed to produce multicellular spheroids mainly for cancer drug discovery[17]. Multicellular spheroids are *in vitro* micro-scale tissue analogs where cell clusters formed by self-assembly. Spheroids harbor several features that make it more physiological platform for early drug discovery due to the following reason: 1) Spheroids multicellular 3D architecture mimic the *in vivo* microenvironment of tumor and extracellular matrix deposition that are found *in vivo* but absent in monolayer culture; 2) Spheroids of *in vivo* solid tumors models develop three different zones of proliferating, quiescent and necrotic cells beside the hypoxia present in many cancers, which have been identified as one of main causes for drug resistance; 3) the tight cell-cell interactions is comparable to those in *in vivo* tissues[18]. Taken together, 3D spheroids provide an improved model for testing *in vitro* siRNA delivery compare to regular monolayer cell culture model.

1.2 Research Objectives

The aim of this study is to develop 3D spheroids of HCT116 colon cancer cell line using the hanging drop method and evaluated NP1, a novel CPP (STR-H16R8) developed by Dr. Chen's group to assist siRNA delivery to silence specific targeted genes for therapeutic purposes.

The overall objectives of this thesis include:

1) Generating 3D tumor micro-tissues using hanging drop method.

2) Demonstrate external morphological and internal histological characterization of generated 3D tumor spheroids.

3) Evaluate the therapeutic potential of CPP (NP1) in assisting siRNA delivery in 2D cell monolayer and 3D spheroids.

1.3 Outline of Thesis

This thesis consists of five chapters. The scope of each chapter is listed as follows:

Chapter1 gives brief introduction of the thesis including, introduction to RNA interference process, potential siRNA therapeutics and limitations, the potential of CPP as siRNA delivery systems, importance of 3D tumor micro-tissues as *in vitro* model for early drug screening. The research objectives and the outline of the thesis are also given.

Chapter 2 presents a review of RNAi working mechanism, current and potential therapeutic applications of siRNAs, current non-viral delivery systems of siRNA including polymeric, lipid based and CPPs.

Chapter 3 lists all materials and methods relevant to this study.

Chapter 4 the results and discussion of this study are stated including, (1) morphological characterization of HCT 116 spheroids; (2) cellular uptake and penetration of NP1-siRNA complexes in tumor spheroids; (3) *in vitro* transfection efficiency*;* (4) cytotoxicity; (5) induced apoptosis; (6) histological evaluation.

Chapter 5 states the conclusions of this study and a proposal for future studies.

Chapter 2
Literature Review

2.1 RNA Interference

At the forefront of revolutionizing medicine, gene therapy provides an effective potential to treat wide range of diseases by regulating defective genes. RNA interference (RNAi) holds great promise as therapeutic agents due to the high efficiency and specific posttranscriptional gene silencing process, which can be triggered by small interfering RNA (siRNA). SiRNAs are a class of 21 to 23 nucleotide-long double-stranded RNA molecules that inhibits the expression of a specific gene by the degradation of its complementary messenger RNA (mRNA)[2]. The efficiency and specificity of this process makes siRNA a potential tool for gene therapy.

2.1.1 Working Mechanism of RNAi

RNA interference (RNAi) is double-stranded RNA molecules, which can interfere with any complementary mRNA sequence and consequently silence the expression of sequence specific gene product in a range of organisms. In general, long dsRNA is the precursor of siRNA, the long dsRNA cleaved into smaller siRNA molecules 21-23 nt by RNase III like enzyme, Dicer, once introduce to the cells[3]. The newly formed ds-siRNA molecules then bind to a protein complex called RNA-induced silencing complex (RISC). Due to the helicase activity of the protein complex siRNA is unwounded into a sense (passenger) strand and an antisense (guide) strand. Guide strand with RISC will be activated and bind to the complementary target mRNA which will be then cleaved and

degraded by enzymatic activity within RISC (argonaute 2)[4–7]. By that the expression of specific gene into protein will be prevented or terminated as represented in Figure 2.1[19].

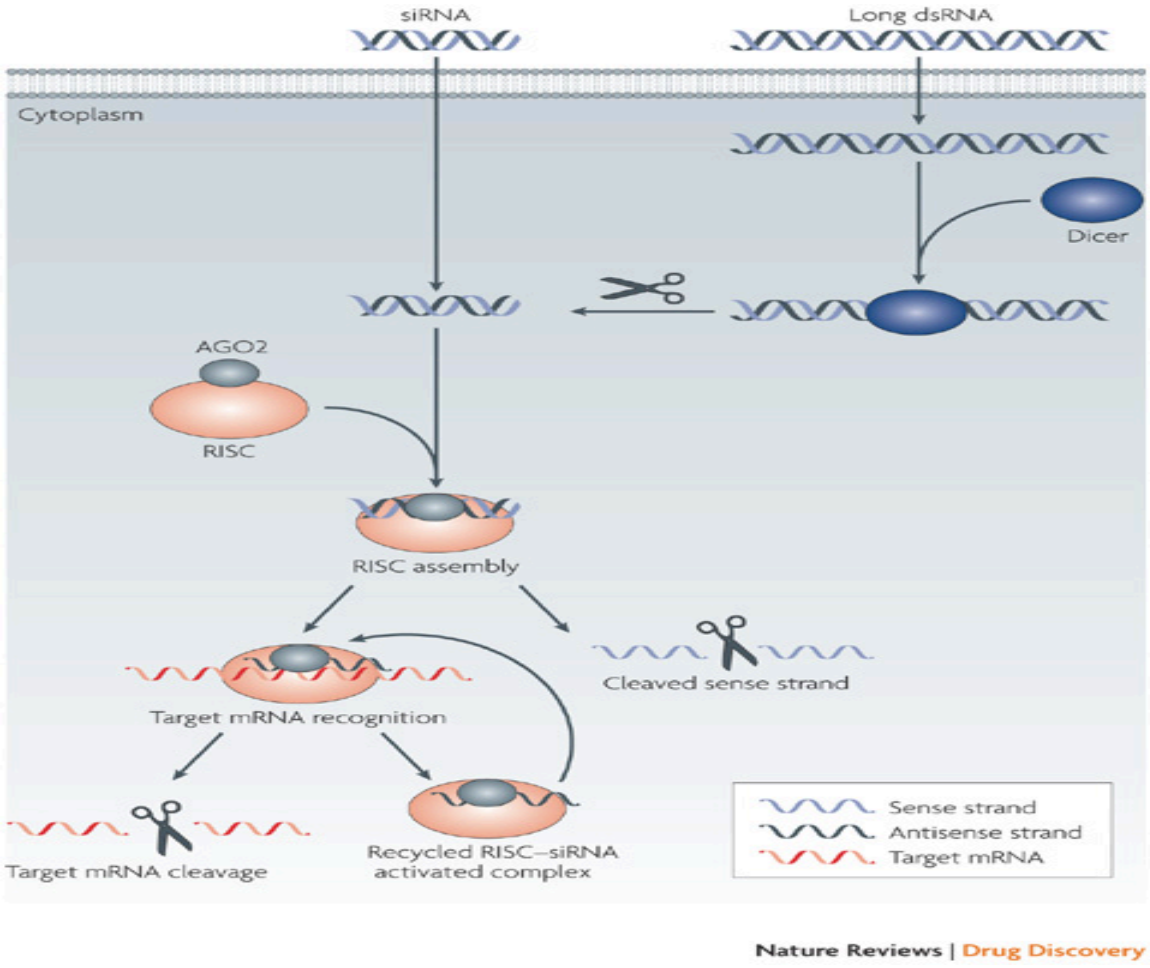

Figure 2.1. A schematic representation of RNAi working mechanism[19]. Reprinted with permission from Nature.

2.2 Therapeutic Potential of RNAi Technology

Since the discovery of RNAi, there has been an explosion of interest in using this technology for basic and applied research mainly in gene therapy and development of gene-specific drugs as RNAi has been one of the most promising new approaches for disease therapy. Recent advances in RNAi therapy have broadened the list of diseases that may be treated by RNAi, including cancers, type 2 diabetes[20], Parkinson's disease[21],

HIV infection[22], HBV chronic infection[23] and hypercholesterolemia[24]. RNAi have been tested in different organs of the body for varies types of diseases either by direct or systematic delivery as shown in Figure 2.2[25]. Interestingly, direct RNAi delivery of siRNA molecules has been carried out successfully to specific tissues and organs such as, eye, skin, lung, nose, the nervous system and the digestive system. On the other hand, systemic RNAi delivery is done through intravenous delivery of siRNA molecules into liver, tumors and lung.

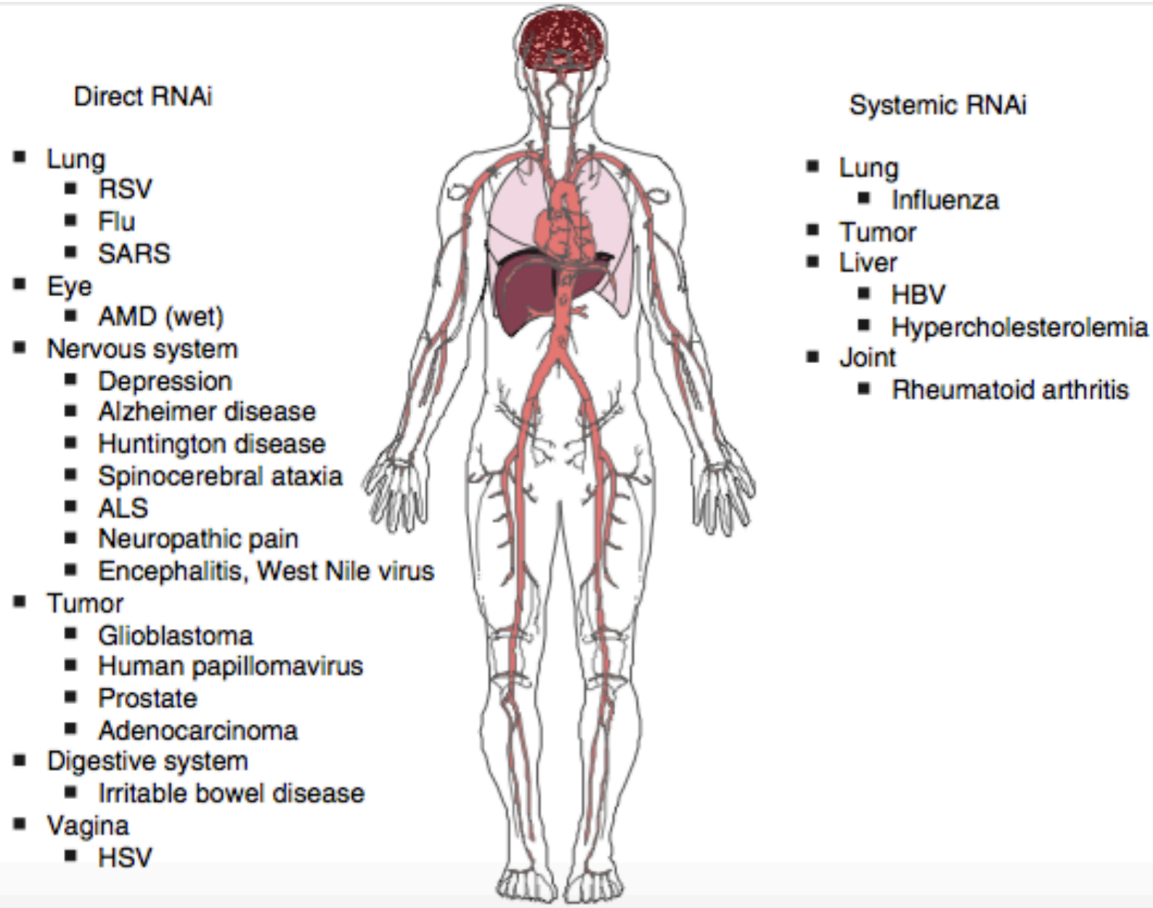

Figure 2.2. Organs and diseases for which the effect of RNAi has been tested by direct and systemic delivery[25]. Reprinted with permission from Nature.

2.2.1 Cancer

Cancer is a leading cause of death worldwide and expected to increase to reach over 13.1 million in 2030[26]. Cancer is a genetic disease, involves different mutations and epigenetic alterations that lead to uncontrollable cell proliferation, division and differentiation[27,28]. siRNA is a powerful tool to silence cancer-related gene targets. Extensive preclinical studies have been conducted on this regard and shown that specific cancer related gene silencing can inhibit tumor cell growth, angiogenesis, metastasis and chemo-resistance[29–31].

Bcl-2 is anti-apoptotic marker over expressed in many human tumors and considered as an important oncogene. Suppression or silencing of Bcl-2 proves to induce apoptosis and reduce the tumor growth[32]. Additionally, angiogenesis is a key factor for neoplasia and metastasis of tumor, vascular endothelial growth factor (VEGF) is involved in the growth of new blood vessels from tumor surrounding tissues providing more nutrients for tumor growth and proliferation. Based on that VEGF pathway is the hottest target of tumor angiogenesis inhibition[33,34].

Moreover, understanding the characteristics of the tumor microenvironment is a key factor for cancer therapy. Hypoxia-inducible factor-1α (HIF-1α) is an attractive therapeutic target that is a key transcription factor during hypoxia and activates the transcription of genes involved in angiogenesis, invasion, cell survival and glucose[35,36]. HIF-1α under hypoxic condition activate the expression of different hypoxia-response genes such as, vascular endothelial growth factor (VEGF)[37].

2.2.2 Infectious Diseases

Many diseases caused by viruses and bacteria such as, HIV Influenza, Hepatitis, pneumonia and sepsis continue to be one major cause of death around the world. RNAi ability to suppress the replication of viruses and other infectious agents has been clearly demonstrated in *in vitro* studies[38].

HIV is a retrovirus that causes acquired immunodeficiency syndrome (AIDS), a chronic and debilitating disease that cannot be cured with current antiretroviral drugs[39]. The pattern, reproduction, and lifecycle of gene expression of HIV are well known and was the first infectious agent targeted by RNAi technology. HIV genome composed of nine viral genes (*gag*, *pol*,*vif*, *vpr*, *tat*, *rev*, *vpu*, *env*, and *nef*) that are essential in all processes of the viral replicative cycle, assembly, entry and receptor binding, membrane fusion, reverse transcription, integration, and proteolytic protein processing. Therefore, studies have been conducted using siRNAs and shRNAs to target and silence these essential genes, table 2.1 represent some potential RNAi targets for HIV therapy[39]**.**

Hepatitis B virus (HBV) is a DNA virus, causing a global health problem with over 350 million carriers worldwide[40]. In fact, HBV is an excellent candidate for therapeutic RNAi, due to the compact genome with no redundancy. Therefore prevents the virus from evading RNAi therapy by mutations and inhibit viral gene expression and replication with higher rate of success[41]. McCaffrey *et al*. reported that plasmids expressing HBV specific short hairpin RNAs (shRNAs) significantly reduced viral mRNAs, HBV surface antigen (HBsAg) and HBV core antigen (HBcAg), thus inhibiting HBV replication in infected mice[42].

Table 2.1. Potential RNAi gene targets for HIV therapy[39]. Reprinted with free access from BioMed Central.

Gene targets	Function of target gene	Type of study
Gag	Proteolytic processing of the HIV-1 genome	Mouse
Pol	Transcription	Mouse
env	Receptor binding and fusion	Phase I/II
tat	Transcription or RNAi modulation	Phase 0
rev	Reverse transcription, integration	Mouse
nef	Immune modulation	Mouse
pol (integrase)	Integration	*In vitro*
pol (reverse transcriptase)	Reverse transcription	*In vitro*
Promoter	Transcription	Mouse
Long terminal repeats	Genome expression	*In vitro*
CCR5	Receptor binding and fusion	Phase 0/phase I/II
CXCR4	Receptor binding and fusion	*In vitro*
CD4	Receptor binding and fusion	*In vitro*
LEDGF/p75	Integration	*In vitro*
Importin-7	Integration	*In vitro*
Chaperonin	Integration	*In vitro*
P-TEFb	Transcription	*In vitro*
Tat-SF1	Transcription	*In vitro*
SPT5	Transcription	*In vitro*
Cyclin T1	Transcription	*In vitro*
DDX3	Export	*In vitro*

SOCS1	Trafficking or immune modulation	*In vitro*
TRBP	Immune modulation or RNAi pathway	*In vitro*
TNPO3	Nuclear entry of viral pre-integration complex	Mouse

2.2.3 Neurodegenerative Diseases

Neurodegenerative diseases are a heterogeneous group of disorders that occurs as a result of degeneration or defect of the central or peripheral nervous system. Typical examples of neurodegenerative diseases are Alzheimer's (AD), Parkinson's (PD), Huntington's (HD) and amyotrophic lateral sclerosis (ALS)[43]. Among all the expensive treatment available for neurodegenerative diseases, RNAi-based therapies have emerged as a promising candidate for treatment and inhibition of related disease genes. Down regulation of p75 neurotrophin receptor[44], pro-apoptotic members of the Bcl-2 family[45] and caspases[46] by RNAi effectively prevent neuronal death.

2.3 RNAi Therapeutics in Clinical Trials

In 2006 RNAi was awarded the Nobel Prize for medicine. Since then, RNAi rapidly advanced from research discovery to clinical trials and billions of dollars have been invested in this field. The number of RNAi based drugs in clinical trials is increasing each year and reach 22 RNAi based drugs by 2013 as listed in table 2.2. Majority of siRNAs based drugs in clinical trails were administered by local delivery, which is not suitable for all types of diseases as still there are limitations of using this technology in clinic to be addressed[47].

Table 2.2. RNAi based drugs in clinical trials[47]. Reprinted with free access from Elsevier.

Drug	Target	Delivery system	Disease	Phase
TD101	K6a (N171K mutation)	Naked siRNA	Pachyonychia Congenita	I
AGN211745	VEGFR1	Naked siRNA	Age-Related Macular Degeneration, Choroidal Neovascularization	II
QPI-1007	CASP2	Naked siRNA	Optic Atrophy Non-arteritic Anterior Ischemic Optic Neuropathy	I
Bevasiranib	VEGF	Naked siRNA	Diabetic Macular Edema	II
SYL1001	TRPV1	Naked siRNA	Ocular Pain, Dry Eye Syndrome	I, II
I5NP	p53	Naked siRNA	Injury of Kidney, Acute Renal Failure	I
SYL040012	ADRB2	Naked siRNA	Glaucoma, Ocular Hypertension	I, II
ALN-RSV01	RSV nucleocapsid	Naked siRNA	Respiratory syncytial virus infections	II
PF-655	RTP801	Naked siRNA	Choroidal neovascularization diabetic retinopathy diabetic macular edema	II
siRNA-EphA2-DOPC	EphA2	LNP	Advanced Cancers	I

Atu027	PKN3	LNP	Advanced Solid Tumors	I
PRO-040201	ApoB	LNP	Hypercholesterolemia	I
TKM-080301	PLK1	LNP	Multiple Cancers	I
ALN-VSP02	KSP and VEGF	LNP	Solid tumors	I
TKM-100201	VP24, VP35, Zaire Ebola l-polymerase	LNP	Ebola-virus infection	I
ALN-PCS02	PCSK9	LNP	Hypercholesterolemia	I
ALN-TTR02	TTR	LNP	Transthyretin-mediated amyloidosis	II
CALAA-01	RRM2	Cyclodextrin NP	Cancer Solid Tumor	I
siG12D LODER	KRAS	LODER polymer	Pancreatic Ductal Adenocarcinoma Pancreatic Cancer	I
RXi-109	CTGF	Self-delivering RNAi compound	Cicatrix scar prevention	I
ALN–TTRsc	TTR	siRNA–GalNAc conjugate	Transthyretin-mediated amyloidosis	I
ARC-520	Conserved regions of HBV	DPC	HBV	I

2.4 Challenges and Limitations of RNAi Therapeutics

Despite the potential value of RNAi technology, number of problems remains as major obstacle to clinical applications of therapeutic siRNAs. Non-specific off-target gene silencing of siRNA is one of the concerns however, it is highly specific to the gene with a complementary sequence compare to the traditional therapeutics[48]. SiRNA duplexes can stimulate the innate immune system and production of cytokines, depending on the siRNA structure and sequence, method of delivery, and cell type[49]. Normally innate immune system gets activated via a Toll-like receptor (TLR) pathway, if TLRs family including TLR-3, TLR-7 and TLR-8 recognize siRNA molecules[50,51].

Additionally, *in vivo* siRNA silencing target gene expression has been a very challenging task due to its large molecule weight, negative charge, hydrophilicity, sensitivity to nuclease degradation and short plasma half-life of less than ten minutes[8]. These unfavorable properties lead to instability of naked siRNA under physiological conditions, rapid excretion, inability to cross target cell membranes and inefficient intracellular release as Figure 2.3 represent some of the barriers that might encounter siRNA in systemic delivery[9]. Therefore, siRNA as a potential therapeutic agent requires efficient and safe delivery that will retain their biological functions. A variety of carriers have been developed to deliver siRNA and maximize its therapeutic effects including viruses[10], lipids[11], polymers[12], dendrimers[13], peptides[14], and nanoparticles[15].

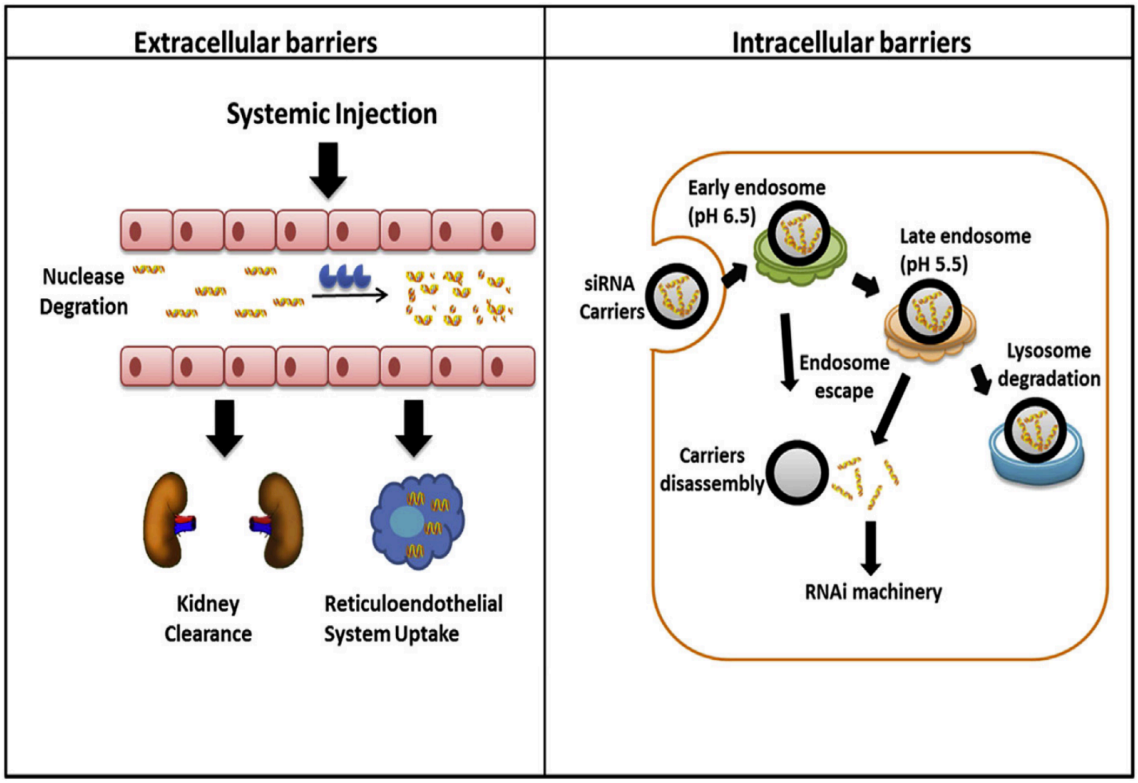

Figure 2.3. Extracellular and intracellular barriers encounter systemically delivered siRNA *in vivo*. After the injection, siRNA may be degraded in the blood stream, rapidly excreted by renal excretion or removed by macrophages. siRNAs may not reach their target cells because of electrostatic repulsion due to the negative surface charge of siRNA and the cell membrane, causing very poor cellular uptake. Once internalized, siRNAs entrapped in endosome-lysosome pathway and may be degraded if fail to escape, leading to poor silencing efficiency as low concentrations of siRNA might reach the cytoplasm to interact with targeted mRNA[47]. Reprinted with free access from Elsevier.

2.5 Current Non-Viral Delivery Systems

2.5.1 Polymeric Carriers:

Wu *et al*. 1987, was the first to introduce the cationic polymers[52], linear or branched cationic polymers made up of repeated units of monomers is one of the widely studied non-viral siRNA delivery systems[53]. The positive charge in polymers drive the interaction with negative charge phosphates of siRNA or DNA through electrostatic force causing siRNA condensation and formation of polyplexes[54].

Generally, the net positive charge increases, as the molecular weight of the synthesized polymers is higher, therefore more stable complexes achieved with tighter binding to the nuclear material[55]. Several polymers, either synthetic or natural, have been designed and used in siRNA delivery: poly-L-lysine (PLL), poly-D, L-lactide-co-glycolide (PLGA), poly-ethyleneimine (PEI), poly-propylenimine (PPI), poly-caprolactone (PCL), poly-d,l-lactide (PLA), and many others. These polymers and their modifications have been investigated both *in vitro* and *in vivo* for siRNAs based therapy[47,54].

For protection of complexes under physiologiacal conditions polymer–siRNA were conjugated with Polyethyleneglycol (PEG), due to its steric stabilization effects, biocompatibility, and anti-fouling properties. One of the examples of this application is production of stable polyelectrolyte complex (PEC) micelles from, siRNA-PEG conjugate complexed with branched polyethylenimine (bPEI, 25 kDa) and KALA peptides. Figure 2.4, illustrate the delivery strategies of different siRNA-polymer complexes depending on the conjugates of siRNAs to the polymers[56].

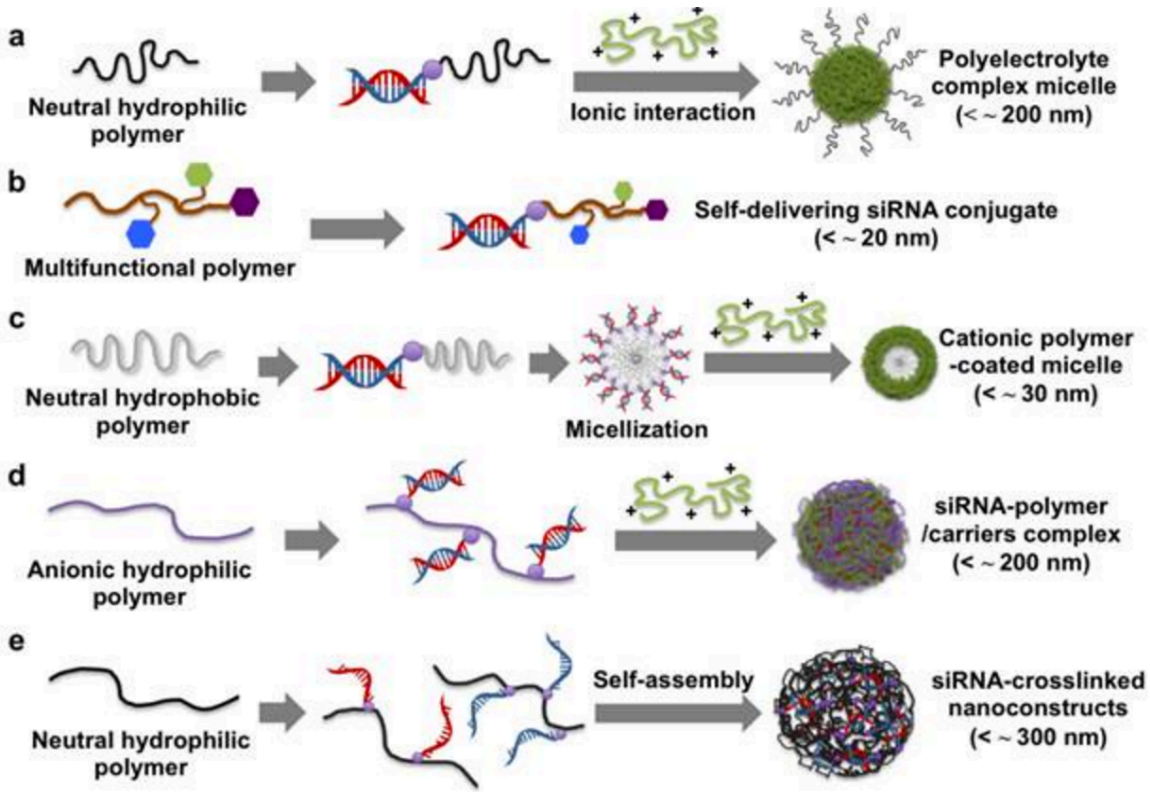

Figure 2.4. Illustration of different delivery strategies of siRNA-polymer complexes[56]. Reprinted with free access from Theranostics

2.5.2 Lipid-Based Carriers

Several classes of lipid-based nanocarriers have been synthesized and studied for siRNA delivery including liposomes, microemulsions, solid lipid nanoparticles, micelles and lipid-based nanocarriers including other materials such as polymers or peptides[57]. Liposomes are globular vesicles, consisting of phospholipid bilayer with an aqueous core[58,59].

Liposomes protect and deliver siRNA by forming Lipoplexes complexes with diameter less than 100 nm, via hydrophobic and electrostatic interactions. The hydrophobic nature is driven from the tails of lipids align inside the lipoplexes, while the

hydrophilic heads align outside in aqueous solutions. Electrostatic interactions formed due to the interaction between the positive charges in cationic lipids and the negatively charge in phosphate backbone of siRNAs[60]. Therefore, cationic lipid based liposomes are most commonly used over neutral lipid liposomes for nucleic acids delivery, including siRNA, plasmid DNAs and oligonucleotides. Strongly constructed complexes with siRNAs are achieved by cationic charge liposomes compare to neutral lipids through electrostatic interactions, and further can facilitate cellular uptake by interacting with negatively charged cell membranes. A number of different cationic liposomes have been developed, including 1-oleoyl-2-[6-[(7-nitro-2-1,3-benzoxadiazol-4-yl)amino]hexanoyl]-3-trimethylammonium propane (DOTAP)[61], N-[1-(2,3-dioleoyloxy)propyl]-N,N,Ntrimethylammonium chloride (DOTMA)[62], cetyl trimethylammonium bromide, dimethyldioctadecylammonium bromide (DDAB), 1,2-dimyristyloxypropyl-3-dimethyl-hydroxy ethyl ammonium bromide-cholesterol (DMRIE-C), 1,2-dioleoyl-*sn*-glycero-3-phosphocholine (DOPC), L-α-dioleoyl phosphatidylethanolamine (DOPE), 3β-[*N*-(*N*′,*N*′-dimethylaminoethane)-carbamoyl]cholesterol(DC-Chol)[63]. Different lipid formulations have been commercialized for *in vitro* transfection including Lipofectamine 2000 (Life Technologies), Oligofectamine (Life Technologies) and TransIT-2020 (Mirus Bio). However, their uses *in vivo* are limited due to high toxicity and poor stability[64].

2.5.3 Cell-Penetrating Peptide Based Carriers

Short peptides typically with 5–30 amino acids, are known as cell penetrating peptides (CPPs), membrane translocation sequences, “Trojan peptides” or protein transduction domains[65]. There are three basic types of CPPs, cationic, hydrophobic and amphipathic

peptides (table 2.3)[66]. HIV-1 protein TAT, was the first discovered cationic CPP[67]. Cationic peptides often consists of arginine, lysine and histidine amino acid sequences which mediate the interaction with anionic/acidic motifs causing a receptor-independent interaction with the cell membrane. Guanidine head group in arginine amino acid facilitate the internalization to the cells by forming hydrogen bonds with the negatively charged phosphates and sulfates on the cell membrane. Lysine is a positively charged amino acid but with out guanidine head group, which lead to less uptake compare to arginine[66]. Futaki *et al*., demonstrated that eight positive charges at least are needed for efficient cellular uptake of cationic CPPs[68].Hydrophobic peptides, consists of hydrophobic amino acid residues with low net charge. Amphipathic CPPs, constructed from lipophilic and hydrophilic building blocks, which mediate the translocation across the cell membrane[69].The main advantages of CPP over other nano-carriers are, low toxicity and immunogenicity, rapid and efficient intracellular delivery[65]. Cationic CPPs, condense siRNA by the electrostatic interactions between negatively charged phosphate backbone of siRNA and positively charged amino acids. The positive net charge on the complex enhances the translocation through the cell membrane[70].

Table 2.3. Sequences and types of some synthetic or chimeric CPPs[66]. Reprinted with permission from Elsevier.

Type	Name	Amino acid sequence
Amphipathic	Transportan	GWTLNSAGYLLGKINLKALAALAKKIL
	Pep-1	KETWWETWWTEWSQPKKKRKV
	MPG	GLAFLGFLGAAGSTMGAWSQPKKKRKV
	pVEC	LLIILRRRIRKQAHAHSK

	MAP	KLALKLALKALKAALKLA
	CADY	GLWRALWRLLRSLWRLLWRA
Cationic	Polyarginine	R8, R9, R10, R12
	TAT 49	RKKRRQRRR
	Penetratin (pAntp)	RQIKIWFQNRRMKWKK
	P22N	NAKTRRHERRRKLAIER
	DPV3	RKKRRRESRKKRRRES
	DPV6	GRPRESGKKRKRKRLKP
Hydrophobic	K-FGF	AAVLLPVLLAAP
	C105Y	CSIPPEVKFNKPFVYLI

2.5.3.1 NP1 (STR-H16R8) Cell Penetrating Peptide

Taking the knowledge that oligoarginine is one of the most widely utilized CPPs for intracellular delivery, is employed as a model carrier due to the positive surface charge and high binding to the surface of cell membrane. Additionally, it has been reported that oligoarginine uptake increases with increasing charges. In order to overcome the lack of silencing activity induced by oligoarginine[71], stearic acid modification and various oligohistidine modifications were introduced to enhance cellular uptake and endosomal escape of siRNA. Moreover, DLS results showed that hydrophobic stearyl groups conjugated to a peptide sequence improve the co-assembly of peptide with siRNA and forming nanoparticles (<200 nm). The residue number ratio of histidine/arginine in a stearylated peptide sequence is critical for inducing pronounced gene silencing, based on that different designs of stearylated and oligohistidylated oligoarginine based siRNA

carriers that have significantly improved efficiency compared to the most commonly used benchmark delivery systems, Lipofactamine 2000 (Lipo). NP1 (STR-H16R8) showed efficient uptake and silencing efficiency. Figure 2.5, demonstrates the whole process of peptide mediated siRNA delivery, from peptide-siRNA binding, internalization, intracellular trafficking, to endosomal release and finally RNA interference[16].

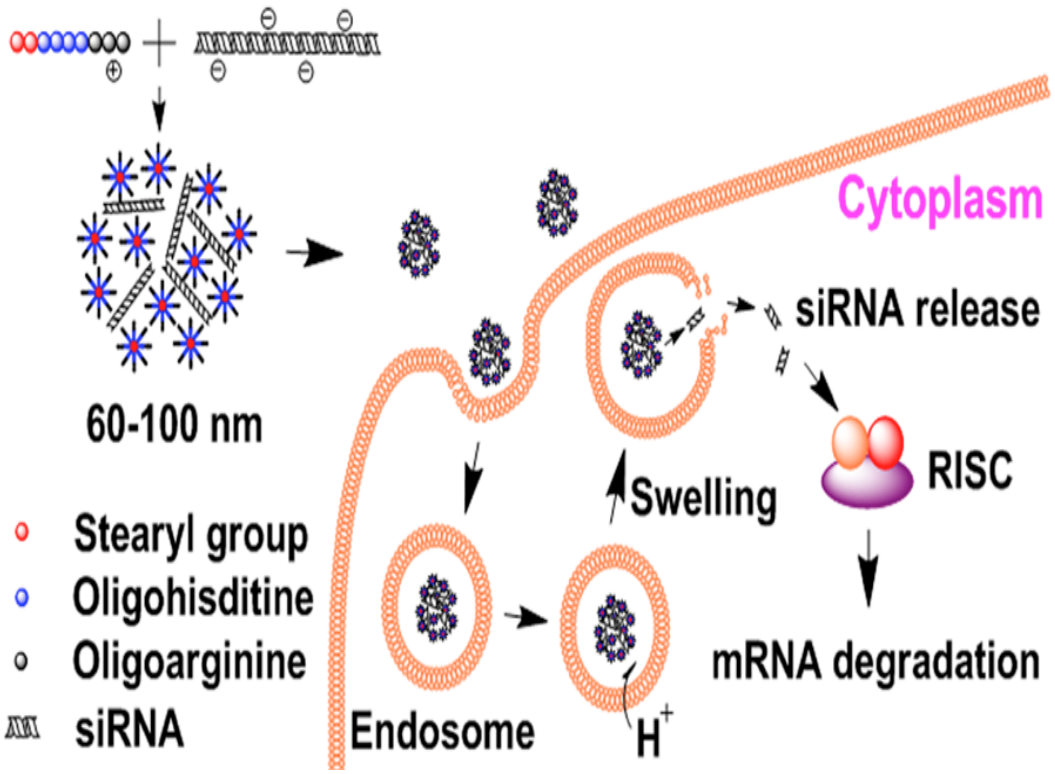

Figure 2.5. Schematic diagram of stearylated oligohistidylated oligoarginine based peptide as siRNA carriers, positively charge NP1 complex negatively charge siRNA in to nanoparticles ranging from 60-100 nm. After the internalization to the cells through endosomal pathway, siRNA can be released from endosome by proton sponge effect where the influx of protons and water increased causing endosome swelling and rupture then siRNA released to the cytoplasm where it can bind to RISC and silence the targeted mRNA[16]. Reprinted with permission from Elsevier.

Chapter 3
Materials and Methods

3.1 Cell Culture

HCT 116 colon cancer cells were purchased from American Type Culture Collection (ATCC CCL-247) and maintained in Dulbecco's Modified Eagle Medium (DMEM) (Thermo Scientific, Ontario, CA) supplemented with 10% fetal bovine serum (FBS) (Sigma-Aldrich, Ontario, CA). The cells were incubated at 37°C in 5% CO_2.

3.2 Preparation of NP1 and NP1-siRNA Complexes

NP1 peptide synthesized by CanPeptide Inc (Quebec, Canada), was prepared by dissolving in RNase free water (Thermo scientific, Ottawa, Canada) at a concentration of 500 μM and stored at -20°C. All siRNAs used in this work were dissolved in RNase free water at a concentration of 50 μM, and were store at -80°C.

NP1-siRNA complexes were prepared in Opti-MEM (Invitrogen, Carlsbad, CA, USA) for transfection experiments at 60/1 molar ratio and final concentration of 100 nM siRNA by slowly mixing the peptide solution into siRNA solution with pipette. Then were incubated at room temperature for 20 min to form the complexes before adding to the cells.

Lipofectamine 2000 (Life Technologies, Carlsbad, USA), a commercial transfection reagent, was used as positive control in experiments. The lipo 2000-siRNA complexes were prepared in Opti-MEM according to the manufacturer protocol instructions and incubated at room temperature for 20 min before adding it to the cells.

3.3 Sequences of siRNAs

Vascular endothelial growth factor A (VEGF A) and hypoxia inducible factor 1, alpha (HIF-1A) were purchased from Life Technologies. The siRNA targeting B-cell lymphoma 2 (Bcl-2) oncogene was synthesized by Sigma, with a sense sequence of 5'-GGT GGG GTC ATG TGT GTG G-dTdT, and antisense sequence of 5'-CGG TTC AGGTAC TCA GTC ATC C-dTdT. The SilencerTM Cy3-labeled GAPDH siRNA was purchased from Ambion, used in fluorescence microscopy and Fluorescence Activated Cell Sorting (FACS). The scrambled siRNA was purchased from Life Technologies (Carlsbad, USA) was used as negative control in the experiments.

3.4 Particle Size Measurement (DLS)

Particle size of NP1-siRNA and Lipo-siRNA complexes were determined by dynamic light scattering on a Zetasizer Nano ZS (Malvern Instruments, Worcestershire,UK) at 25°C in transparent ZEN0040-disposable microcuvette cells (40 µl). Samples were prepared in RNase-free water as described before for complexes formation and allowed to stabilize for 20 min at RT. Three measurements were performed to generate the intensity-based size.

3.5 Generation of Tumor Spheroids from HCT 116 cells

When HCT116 cells reach 85% confluency or greater, the cells were detached with trypsin/EDTA and counted using a haemocytometer to seed around 2500 cell/well. Dead cells were excluded from counting using 75% (v/v) trypan blue stain exclusion. HCT 116 3D spheroids were generated in 3D hanging drop plate (3D Biomatrix) where around 40 µl of cell suspension was loaded in each well with initial seeding density of 2500

cell/well. Cells were cultured in DMEM supplemented with 10% (v/v) fetal bovine serum and incubated at 37°C in a humidified atmosphere containing 5% CO_2. HCT 116 cells require at least 3 days to form compact spheroids.

3.6 Light Microscopy

Morphology of HCT 116 3D spheroids was observed by light microscopy (EVOS fl digital inverted microscope). The diameter of the spheroids was measured using image J software.

3.7 Scanning Electron Microscopy (SEM)

HCT 116 cells were seeded at 2500 cells/well in a 96-well hanging drop plate (3D Biomatrix) and incubated at 37ºC in a humidified atmosphere with 5% CO_2 as described before. Then 3D spheroids were let to form and collected at different incubation times at day 5, 7 and 10. The spheroids were then washed with PBS twice, then cells were fixed by adding100 µl of 5% Glutaraldehyde (v/v, dissolving in PBS) and incubated at 4ºC overnight. After that, the fixative was discarded and the cells were washed twice with PBS. Spheroids then were loaded on a silicon wafer and dehydrated with gradient concentrations of Ethanol series (10% to 100%). Finally, the spheroids were allowed to air dry at room temperature, then imaged using ESEM at 10 kV without gold coating.

3.8 Fluorescence-Activated Cell Sorting (FACS)

3.8.1 Cy-3 GAPDH Uptake Efficiency

3.8.1.1 Uptake Efficiency in Monolayer Cell Culture

The cellular uptake of NP1-Cy3-labeled GAPDH siRNA complex was studied using flow cytometry (type BD Biosciences, BD FACS Vantage SE Cell Sorter, USA). HCT 116 cells were seeded in 24-well plates with initial seeding density around 80000 cell/well and incubated at 37°C in a humidified atmosphere containing 5% CO_2 for 24 hours. Cells then transfected with NP1-Cy3-labeled siRNA complexes at molar ratio 60/1 with final concentration of 100 nM siRNA/well and incubated for 3 hours at 37°C, cells were then rinsed twice with PBS. Followed by detachment of the cells from the plate with 0.25% trypsin/EDTA, and then collected in the suspension of 4% Paraformaldehyde (PFA) in PBS. Samples were analyzed by fluorescence activated cell sorting (FACS), and the data were analyzed by Flowjo software.

3.8.1.2 Uptake Efficiency in 3D Spheroids

3D spheroids of HCT 116 cells were formed by seeding 2500 cells/well in a 96-well hanging drop plate (3D Biomatrix) and incubated at 37ºC in a humidified atmosphere with 5% CO_2 for 5 days. At day 5, 10 µl of Opti-MEM that contain NP1-Cy3-labeled siRNA complexes at molar ratio 60/1 with final concentration of 100 nM siRNA/well was added and incubated for 3,6,24 and 48 hours. Then, spheroids were collected and washed twice with PBS. Afterwards, spheroids were dissociated into single cell suspension by adding 500 µl Accumax (Sigma) then incubated for 30 minutes at 37°C. After 15 minutes spheroids were dissociated mechanically by pipetting up and down. The digestion was stopped by adding a complete cell culture medium, then the cells were

centrifuged and washed twice with PBS. Cells then were collected in 500 µl 4% PFA and analyzed as described before.

3.8.2 Induced Apoptosis

Spheroids were harvested 96 hours post transfection with siRNA-NP1 complexes and transferred to ependrof tubes followed by washing with PBS twice. Afterwards, spheroids were dissociated into single cell suspension by adding 500 µl Accumax (Sigma) then incubated for 30 minutes at 37°C. After 15 minutes spheroids were dissociated mechanically by pipetting up and down. The digestion was stopped by adding a complete cell culture medium, then the cells were centrifuged and washed twice with PBS. 2D monolayer cell were seeded in 24-well plates with initial seeding density around 35000 cell/well and collected 48 hours post transfection. For evaluation of induced apoptosis by Apoptosis Kit with Annexin V FITC and PI, flow cytometry, cells were stained with 4 µl Propidium Iodide (PI) and 5 µl Annexin V. Staining performed in 100 µl Annexin Binding for 15 min at RT then cells analyzed by FACS immediately. Each data measurement was made up from 16 spheroids, repeating the whole procedure independently three times.

3.9 Confocal Laser Scanning Microscopy (CLSM)

3D spheroids of HCT 116 cells were formed by seeding 2500 cells/well in a 96-well hanging drop plate (3D Biomatrix) and incubated at 37ºC in a humidified atmosphere with 5% CO_2 for 5 days. At day 5, 10 µl of Opti-MEM that contain NP1-Cy3-labeled siRNA complexes at molar ratio 60/1 with final concentration of 100 nM siRNA/well

was added and incubated for 24 hours. Thereafter the spheroids were collected and washed twice with PBS, then fixed with 4% Paraformaldehyde (PFA) for 30 min at RT. Fixed spheroids were washed with PBS twice then transferred to a chamber slide. At the end DAPI (Sigma-Aldrich, Oakville, Canada) was added to stain the nuclei of cells and then spheroids were covered by fluoromount aqueous medium. Images were taken with Zeiss LSM 700 confocal microscope.

For further morphological characterization of 3D spheroids, LIVE/DEAD Viability/Cytotoxicity Kit (calcein AM and ethidium homodimer (EthD-1), Invitrogen) was used. Calcein AM is a cell permeant dye used to stain live proliferating cells mainly the outer layer of the spheroid. In proliferating cells, the non-fluorescent calcein AM is converted to a green-fluorescent due to presence of intracellular esterases that will hydrolysis acetoxymethyl ester. Dead cells with disrupted cell membrane were stained by EthD-1which will bind to the DNA and emit red fluorescence. HCT 116 cells were seeded at 2500 cells/well in a 96-well hanging drop plate (3D Biomatrix) and incubated at 37ºC in a humidified atmosphere with 5% CO_2 for 5 days. Then spheroids were collected and washed twice with PBS and LIVE/DEAD Viability/Cytotoxicity Kit was applied per manufacturer's instruction. Thereafter, spheroids were incubated for 1 hour at 37ºC in a humidified atmosphere with 5% CO_2 and washed twice with PBS and fixed with 4% Paraformaldehyde (PFA) for 30 min at RT followed by PBS washing. Fixed spheroids were transferred to a chamber slide and covered by fluoromount aqueous medium. Finally, images were taken with Zeiss LSM 700 confocal microscope.

3.10 Cytotoxicity

3.10.1 Cytotoxicity in 3D Spheroids

3D spheroids of HCT 116 cells were formed by seeding 2500 cells/well in a 96-well hanging drop plate (3D Biomatrix) and incubated at 37ºC in a humidified atmosphere with 5% CO_2 for 72 hours. 10 µl of Opti- MEM that contained samples was added to the cells and incubated for 48 hours. Then spheroids were transferred to a clear, round bottom standard 96-well plate by dropping down the hanging drops, the cytotoxicity of each treatment was determined by the WST-1 assay according to manufacturer protocoled. Cell viability assessed by measuring the absorbance at 450 nm with a plate reader (FLUOstar OPTIMA, BMG, Germany); each treatment included 6 spheroids and results normalized to the non-treated group.

3.10.2 Cytotoxicity in 3D Spheroids

HCT 116 cells were plated in to 96-well plates with initial seeding density around 8,000 cells/well in DMEM medium supplemented with 10% FBS and incubated at 37ºC in a humidified atmosphere with 5% CO_2. 24 hours later, the medium was removed and washed with PBS, and then 50 µl Opti-MEM medium that contained samples was added to the cells. 3 hours later, 50 µl DMEM medium with 30% FBS was added. After incubation for 24 hours at 37°C in a 5% CO_2 atmosphere, the cells were washed with PBS and then 100 µl of Opti-MEM medium containing CCK-8 reagent was added. Cell viability assessed by measuring the absorbance at 570 nm with a plate reader (FLUOstar OPTIMA, BMG, Germany); results were averaged and normalized to the non-treated group.

3.11 *In Vitro* Gene Silencing Efficiency

HCT 116 cells were seeded in a 24-well cell culture plate (40,000/well) for 2D culture and 2500 cell/well in 96 hanging drop plate for 3D culture, in DMEM medium supplemented with 10% FBS. 2D cell monolayer culture incubated for 24 hours, then the medium was removed and washed with PBS and 200 µl Opti-MEM was added to each well. Next, cells were transfected with different complexes of NP1-siRNAs prepared in Opti-MEM with final siRNA concentration of 100 nM. 3 hours later, 300 µl of DMEM with 20% FBS was added, then cells were incubated for 48 hours at 37 °C in a 5% CO_2 atmosphere. For 3D culture, spheroids formed in 3 days were transfected with different complexes of NP1-siRNAs prepared in Opti-MEM with final siRNA concentration of 100 nM and incubated for 96 hours at 37 °C in a 5% CO_2 atmosphere.

For qRT-PCR analysis, the total RNA was extracted from monolayer cells and spheroids with TRIzol extraction method; first TRIzol reagent was added (Life Technologies, Carlsbad, USA), then treated with chloroform (Sigma, Oakville, Canada) and 2-propanol (Sigma-Aldrich, Oakville, Canada) as recommended by the manufacturer. Nanodrop spectrophotometer ND-1000 (Thermo scientific, Ottawa, Canada) was used to measure RNA concentrations. All RNAs were reverse transcribed with Bio-Rad iScript cDNA synthesis kit (Bio-Rad, Mississauga, Canada) according to the manufacturer's protocol. Then, PCR was performed with Brilliant II fast SYBR Green QPCR Master Mix (Agilent Technologies, Wilmington, DE, USA) using an Mx3005PTM real time PCR System (Agilent Technologies, Wilmington, USA). Bcl-2 primers used in this experiment are: 5'-GGT GGG GTC ATG TGT GTG G-3' (F), and 5'-CGG TTC AGG TAC TCA GTC ATC C-3' (R) (Sigma, Oakville, Canada). VEGF primers used in this

experiment are: 5'- CCATGAACTTTCTGCTGTCTT-3' (F), and 5'-ATCGCATCAGGGGCACACAG-3' (R) (Sigma, Oakville, Canada). Cyclophilin, a house-keeping gene, was used as an internal control to normalize the Bcl-2 and VEGF-A gene expressions, with primer sequences as: 5'-GGTGATCTTTGGTCTCTTCGG-3' (F), and 5'-TAGATGCTCTTTCCTCCTGTG-3' (R) (Sigma, Oakville, Canada).

3.12 Western Blot Assay

3.12.1 Protein Extraction and Quantification

Treated spheroids were harvested and washed with cold PBS twice then lysed using 1X cell lysis buffer (100µL) containing proteinase inhibitor (Sigma, USA). Cells were vortexed until lysed and the total protein lysates were collected and stored at -80°C until further analysis.

For protein quantification, protein standard curve was generated using bovine serum albumin (BSA) (Sigma). BCA working solution was prepared by mixing BCA solution I (BCA, Sigma) with solution II (copper sulfate, blue, 4%) at a ratio of 50:1. Then, 10 µl of samples and standard curve were added to a 96 wells plate, and 200 µl BCA solution to each well and incubated at 37^{o}C for 30 min in dark. The estimated protein concentrations were measured using a plate reader (FLUOstar OPTIMA, BMG, Germany) at 560 nm.

3.12.2 SDS- PAGE Gel Preparation

Polyacrylamide gels (12%) were prepared as indicated in table 3.1.

Table 3.1. (12%) Polyacrylamide gel ingredients and corresponding volumes.

2 x 1.5 mm thickness gels	**Stacking**	**Resolving (12%)**
30% acrylamide	975 µl	6.0 ml
0.5 M Tris-HCl pH 6.8	1.875 ml	-
1.5 M Tris-HCl pH 8.8	-	3.75 ml
10% SDS	75 µl	150 µl
H_2O	4.69 ml	5.25 ml
TEMED	15 µl	7.5 µl
10% (APS)	37.5 µl	75 µl

3.12.3 Western Blotting

For electrophoresis, four volumes of sample (20 ug of protein) were mixed with one volume of solubilizing buffer containing 50% glycerol, 7.5 % of SDS, 50 mM Tris, (pH 6.8), 2 mM EDTA, 200 mM dithiothreitol (DTT), and 0.2% of brilliant blue. Proteins were denatured at 95^0C for 5 min and then subjected to SDS-PAGE on a 12% resolving gel using the system of Laemmli. Following electrophoresis, proteins were electrically transferred on a PVDV membrane (Bio-Rad Laboratories, USA) in a semidry transfer system (Turbo System) in a buffer containing 20% ethanol. After transfer, membrane was cut into two parts and blocked with 5% BSA blocker in 1xTBST for 1 hour at room temperature (RT). The higher part was used to detect B-Actin and the lower part is for determining Bcl-2. Subsequently, rabbit anti human Bcl-2 primary antibody and anti-B-Actin primary antibody (Pierce Biotechnology, Rockford, IL, USA) solutions made in 5% blocking reagent was incubated with corresponding membranes at 4^0C for overnight

(table3.2). Before detecting protein bands with chemiluminescent method, the membranes were washed for 5 times with 1xTBST at RT.

Table 3.2 Dilution factors of primary and secondary antibodies.

Primary Antibodies	Dilution	Secondary Antibodies	Dilution
Bcl-2	1:3000	Anti-rabbit	1:10000
B-Actin	1:10000	Anti-rabbit	1:10000

3.13 Histological Evaluation

For histological evaluation spheroids were generated and transfected as described before. Spheroids then were collected and rinsed twice with PBS and processed for staining.

3.13.1 Routine H&E Staining

The spheroid samples were fixed in 10% neutral buffered formalin, centrifuged then embedded in Histo-Gel and routinely processed. The samples were then embedded in paraffin wax. Thereafter, paraffin blocks were serially sectioned in 5 μm thick sections and stained with hematoxylin and eosin (H&E). The histological slides were evaluated using bright field microscopy (Leica DM1000, ICC50 HD, Leica Microsystems Inc, Canada).

3.13.2 Immunohistochemichal Analysis for Proliferation Marker Ki-67

Consecutive 5-μm-thick sections from the paraffin embedded samples, were placed on positively charged slides and immunohistochemically stained with polyclonal rabbit

antibody to detect the proliferation marker Ki-67 (dilution 1:100, Abcam, USA), using the standard avidin-biotin complex method. Tissue slides were deparaffinized with xylene and graded alcohols, then rehydrated with distilled water. Endogenous peroxidase activity was blocked, by placing the slides in 0.5% hydrogen peroxidase/methanol for 10 min followed by a tap water rinse. Background staining was reduced, by incubating slides in 0.3% bovine serum albumin/Tris-buffered saline. Antigen retrieval entailed by placing the slides in a pressure cooker with an antigen unmasking solution (0.01M citrate buffer, pH 6.0) for 1 min. Slides were subsequently incubated with the primary (4°C overnight), then biotinylated secondary antibodies and streptavidin-biotin peroxidase. Additionally, 0.05% 3'3' diaminobenzidine (DAB) was used as chromogen, followed by counterstaining with hematoxylin. The histological slides were evaluated using bright field microscopy (Leica DM1000, Leica Microsystems Inc, Concord, ON).

Chapter 4
Results and Discussion

4.1 Morphological Characterization of HCT 116 Spheroids

The HCT 116 colon cancer cells spheroids were formed using the hanging-drop method. After seeding the cells in the hanging drop plate, the cells in medium suspension tend to aggregate in the bottom center of the hanging droplet and self assemble into spherical micro-tissues (3D spheroids) with time. Optimization of the seeding density and optimal culturing condition was the main step to form consistent spheroids in all the 96 well plate and most important, generating spheroids that have the requirement to mimic the micro-environment of tumors *in vivo*.

Based on previous reports, spheroids with radii of 200 μm and larger will develop three different zones of proliferating cells on the outside, quiescent cells on the inside and necrotic core due to nutrient and oxygen transport limitations[18]. Therefore, seeding density was optimized to generate spheroids with diameter ranging from 200-300 μm. Initial seeding density of 2500 cell/well was the optimal density for HCT 116 cells with an average diameter of ~ 275 μm, at day 4.

Figure 4.1 shows the formation of spheroids, from single cell suspension to compact spheroids. The time required to form compact spheroids depends on the cell line used, some cell lines fail to form compact spheroid by self assembly, addition of hydrogels or collagen to enhance the cell-cell interaction and formation of extra cellular matrix (ECM) is required. HCT 116 cells used in this study, formed compact spheroids by self assembly only as fast as day 3 after seeding with good spherical morphology and consistency among the 96 wells.

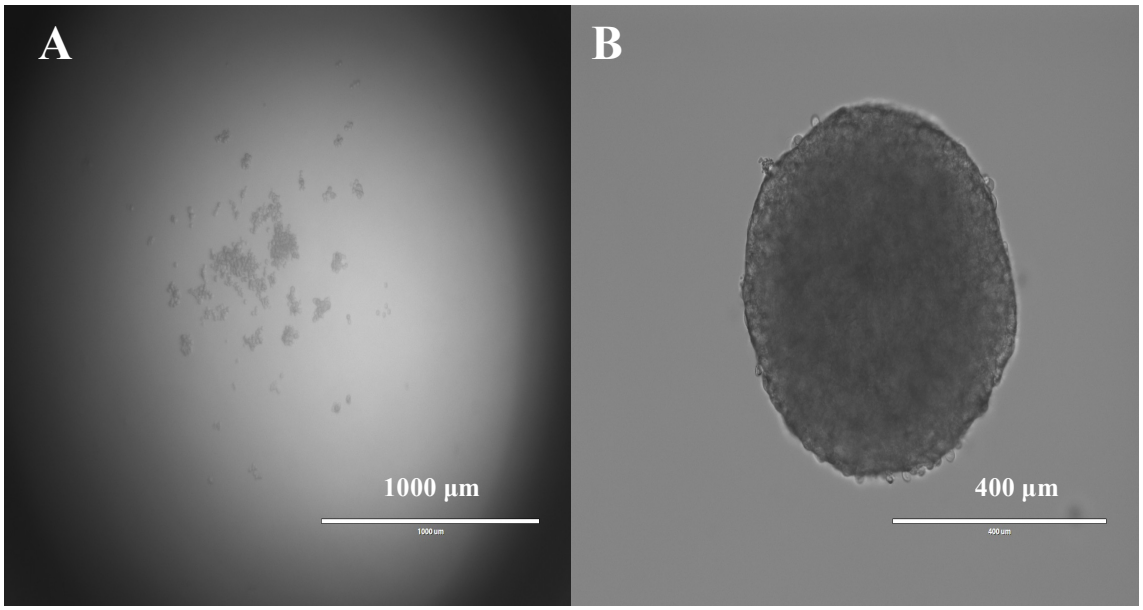

Figure 4.1. Formation of 3D spheroids in the hanging drop plate. (A) Day one post seeding. Cells in the hanging drop tend to aggregate due to the gravitational force. (B) Day six post seeding. HCT 116 cells form compact spherical micro-tissues within three days by self-assembly of cells driven by the gravitational force and cellular interaction that enhance the formation of ECM.

Spheroids in the hanging drop could be maintained for up to 20 days by changing the culturing medium each three days to maintain healthy cells, where 10 µl was sucked out and new 10µl fresh medium added. Under the optical microscopy, the size of spheroids was increasing with the culturing time. Furthermore, to investigate the effect of the culturing time in the morphology, integrity, and volume growth kinetics of the spheroids; MCTS of HCT 116 cells were observed under scanning electron microscope as shown in Figure 4.2.

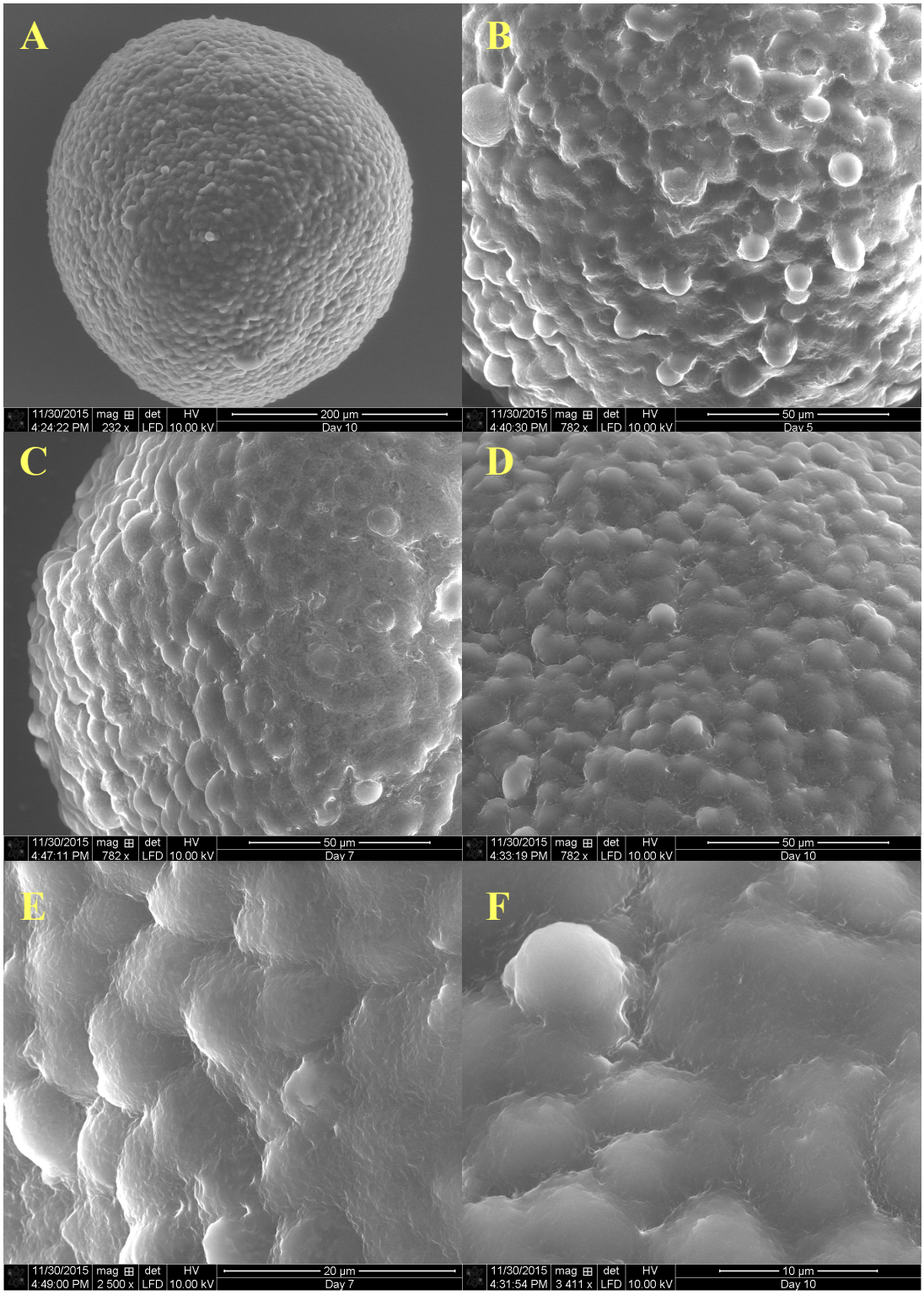

Figure 4.2. Morphological characterization of HCT 116 spheroids under SEM microscope. (A) The overall spherical morphology of compact spheroids, cells

interconnect with one another forming a 3D MCTS. Spheroids cultured for 5 days (B), for 7 days (C), for 10 days (D). The cell-cell interconnection is responsible for the densely packed organization of the spheroids and presence of ECM produced by the cells. With longer culturing time, the compactness, production of ECM and cell interconnection were more pronounced. (E&F) closer look at the cell surface of spheroids collected at day 7 and 10 respectively.

However, the spheroids were generated in scaffold free medium, the cells were able to produce ECM, the hairy like structure between the cells as shown in Figure 4.2 and more appearing at day 5 spheroids. Cancer cells are known to create their own tumour microenvironment, tumour cells interaction with ECM is bidirectional toward progression or inhibition of tumourigenesis. Therefore, development of novel therapies that take in consideration the importance of tumour microenvironment and ECM is highly rational. Generally, ECM is a 3D network of macromolecules that provide scaffolding to support tissue architecture and integrity, including: collagens, elastin, proteoglycans (PGs), hyaluronan (HA), and other non-collagenous matrix glycoproteins[72,73]. Concluding that with longer culturing time, the cells produced more ECM that held cells together through the spheroid and enhance the compactness and integrity.

Furthermore, LIVE/DEAD Viability/Cytotoxicity kit was used to investigate the internal status of the spheroids. As shown in Figure 4.3, cells within the spheroids are divided into three distinct layers. First, cells emitting green fluorescence in the outer live proliferative rim of the spheroid. The outer layers of the cells in the spheroid are in direct contact with the culturing medium and receive all the essential nutrient and oxygen required for normal cell growth and proliferation. Second, the middle layer in the

spheroid, cells not emitting any florescence as the staining used in the kit specific for proliferative and dead cells. These cells are not taking any staining are known as quiescent cells that mean the cells are dormant, live but not dividing as normal cells, where the cell cycle is arrested at G0 or G1. Last, the inner necrotic core of the spheroid, cells are emitting red florescence. Most cells in the spheroid core are dead, due to the limit of nutrient and oxygen supplies compare to the outer layer. Gradient diffusion of oxygen, nutrient and waste and formation of different layers of cells is one of the features of solid tumor microenvironment *in vivo*[74–76].

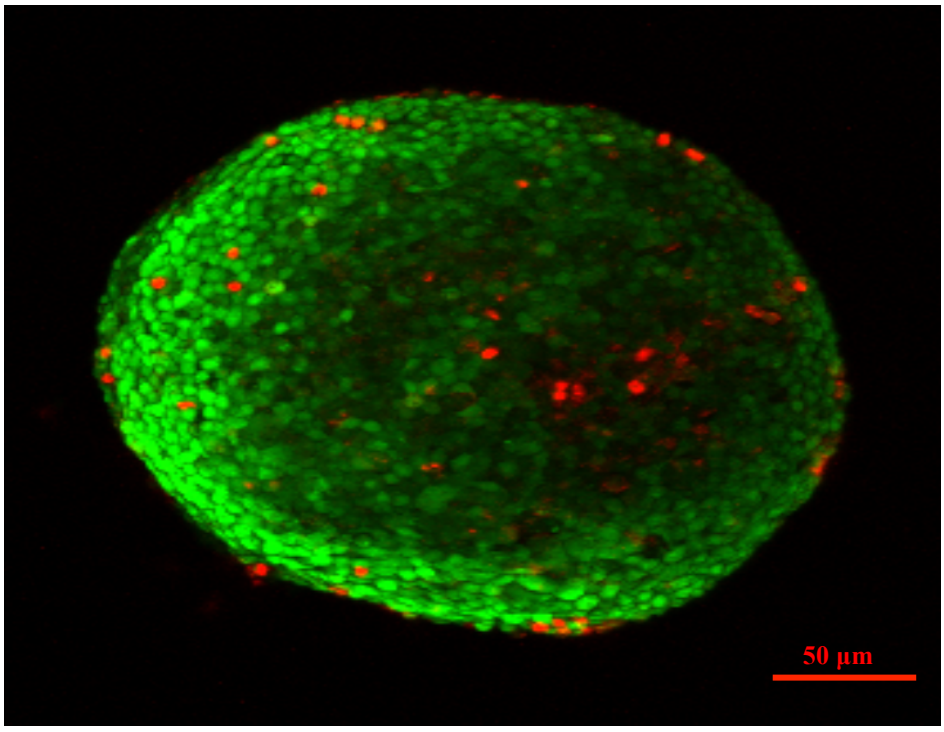

Figure 4.3. Under confocal laser microscope, spheroid was stained with Live/dead assay. Live proliferative cells emitted green fluorescence and dead cells emitted red fluorescence. Non-stained cells are quiescent, live but not dividing cells.

4.2 Cellular Uptake and Penetration of NP1-siRNA Complexes in Tumor Spheroids

Uptake efficiency into the targeted cells is an essential factor for any drug or gene carrier. The effectiveness of NP1 as a carrier for siRNA delivery was determined by measuring the mean fluorescence intensity of cells after delivery of Cy-3 labeled GAPDH siRNA by fluorescence activated cell sorting (FACS). Figure 4.4.A, the mean fluorescence intensity of HCT 116 cells after 3 hours transfection with Cy-3 labeled siRNA complexed with NP1 peptide at molar ratio (60/1) and (100 nM) siRNA, shows a large amount of uptake. Clear evident of significantly higher siRNA delivery efficiency than a market leader Lipofectamine 2000. The rapid and efficient uptake of NP1-siRNA complexes is possibly due to the ability of the cationic peptide NP1 (STR-H16R8) to electrostatically complexes with the anionic siRNA to produce a positively charged complex that has a sufficient stability to allow efficient intracellular delivery of siRNA. The sequence of the peptide effect the cellular internalization of the complexes where polyarginine, optimal length from 5 to 11 residues, is one of the most widely utilized CPPs for intracellular delivery, is employed as a model carrier due to the positive surface charge and high binding to the surface of cell membrane[77].

Furthermore, the penetration of siRNA within tumor spheroids was investigated after 3,6,24 and 48 hours post transfecting the spheroids with NP1-Cy3-labeled GAPDH siRNA. Fluorescence activated cell sorting (FACS) analysis of HCT 116 spheroid cells, gated for live cells (Figure 4.4.B) showed the uptake was time dependent where the uptake is very low in 3 hours and increase with longer times. The uptake in 3 hours in 3D spheroids is significantly lower than that in 2 D cell monolayer. The different cell physiology and culture models possibly affect the uptake efficiency and caused this

difference. Cellular internalization of peptide-siRNA in spheroids was affected by presence of the ECM and the high interaction of the cells in 3D dimension as shown in (Figure 4.2). Therefore, the limited intercellular spaces slowed down the uptake. Surface area is another factor, in 2D monolayer the complexes are in direct contact having higher surface area, where in 3D only the outer layer of the cells are exposed directly. Additionally**,** due to mass diffusion limitation within the spheroid the internalization was reduced and slower than in 2D monolayer cells. This reduced internalization mimic the multicellular drug resistance observed in solid tumors *in vivo*[78]. Moreover, the physicochemical characteristics of the carrier, including the surface charge, size and shape interfere with penetration in the spheroids. Ma H. *et al*, reported that anionic nanoparticles had greater penetration into HeLa spheroids than cationic, and that is opposite in monolayer cells. Possibly, positively charged nanoparticles were preferentially retained by negative surface charges on ECM and taken up by proliferating cells in the outer layer of the spheroids, whereas without any interference the negatively charged nanoparticles diffused into the spheroids[79]. Beside that, smaller nanoparticles penetrated more deeply than larger nanoparticles with the same charge[80].Taken together, NP1 as a cationic peptide with relatively small particle size when complexed with siRNA, ranging from 60-100 nm, these factors could facilitate sufficient siRNA uptake in monolayer and within spheroids (Figure 4.4.C) but with slower pattern.

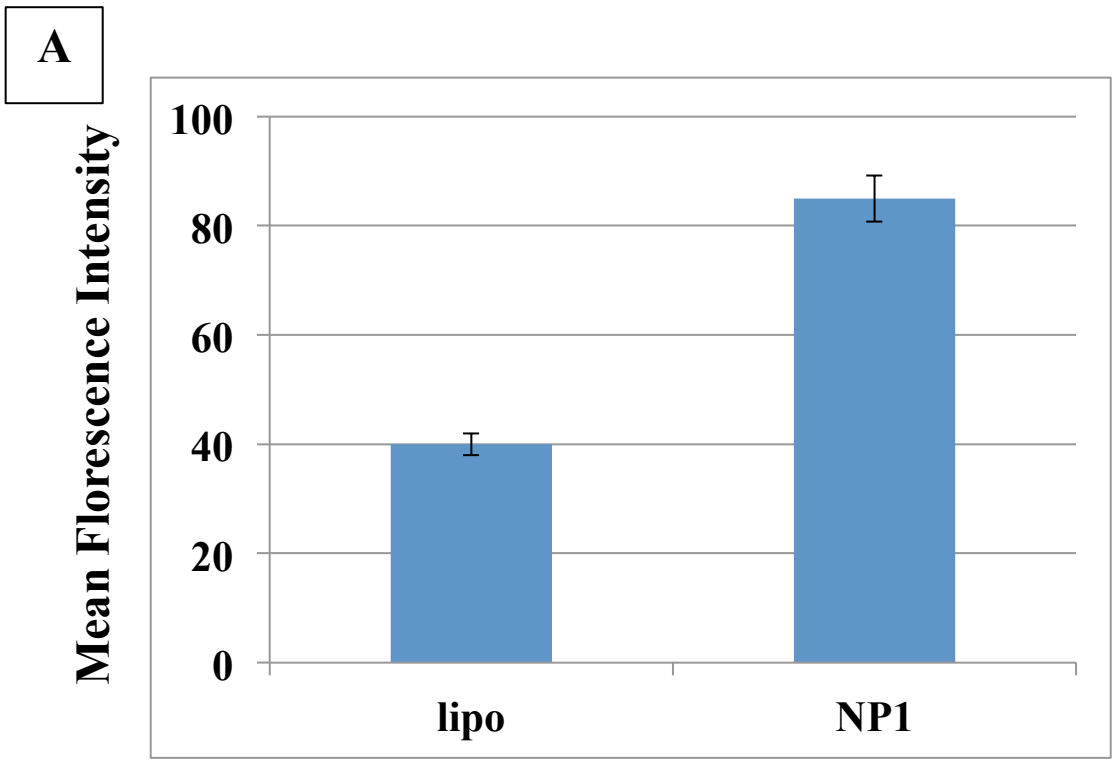
A
Mean Florescence Intensity
100
80
60
40
20
0
lipo
NP1

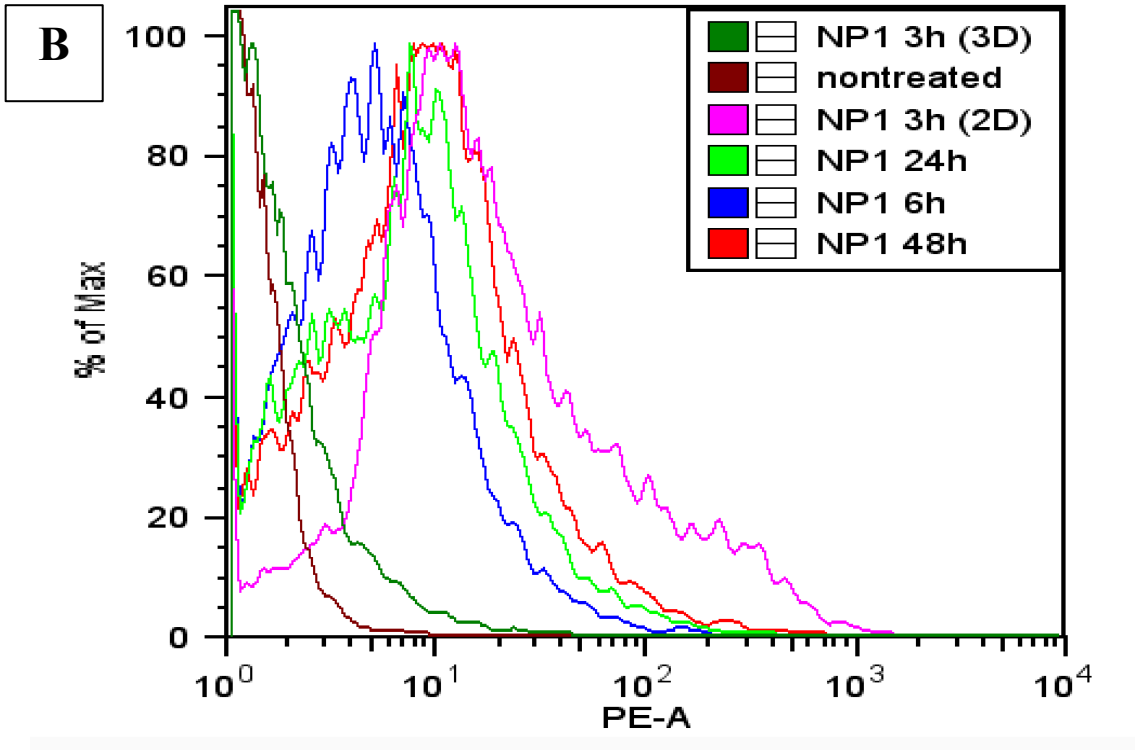
B
% of Max
100
80
60
40
20
0
10^0
10^1
10^2
10^3
10^4
PE-A
NP1 3h (3D)
nontreated
NP1 3h (2D)
NP1 24h
NP1 6h
NP1 48h

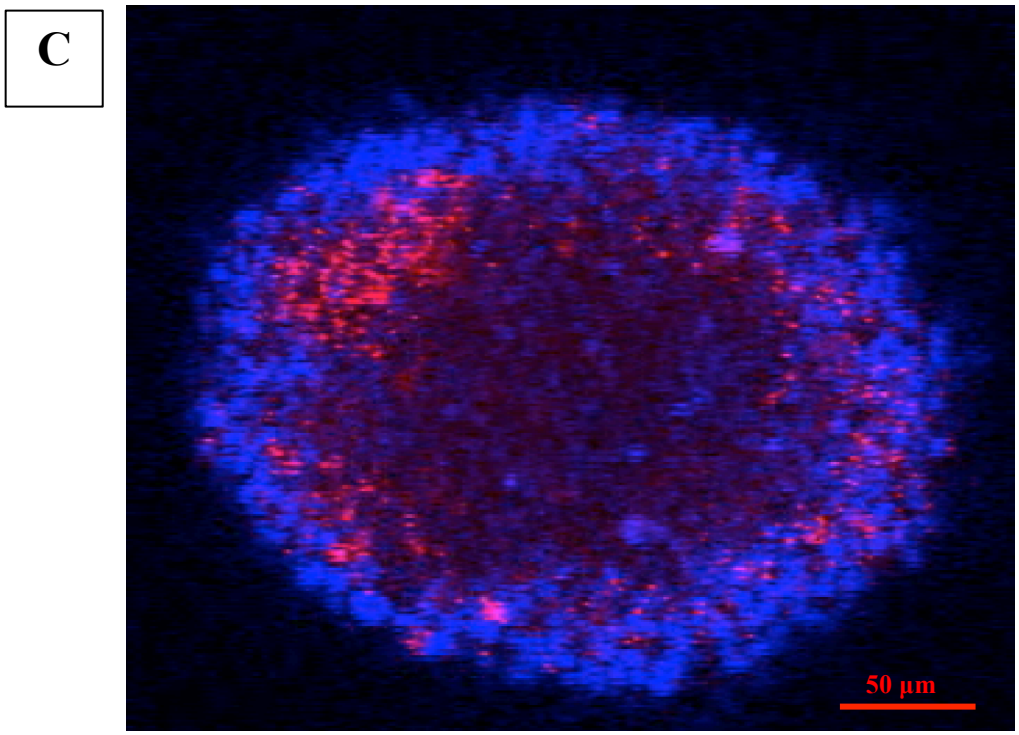

Figure 4.4. Uptake efficiency of NP1-Cy3-labeled GAPDH siRNA. **(A)** Mean fluorescence intensity of Cy3 siRNA in HCT 116 cells treated with NP1-Cy3-labeled GAPDH siRNA for 3 h. The cells were then analyzed by fluorescence activated cell sorting (FACS) in the Cy3 channel. (B) Cellular uptake of NP1-Cy3-labeled GAPDH siRNA in 3D spheroids collected after 3,6,24 and 48 hours post transfection. (C) Penetration of NP1-Cy3-labeled GAPDH siRNA complexes into HCT 116 spheroids 24 hours post treatment. Cell nuclei were stained with DAPI, a nuclear stain emitting blue fluorescence after excitation, and Cy3 (Cy3-labeled GAPDH siRNA) emitting red fluorescence after excitation. Results are expressed as mean ± standard deviation (n=3).

4.3 Cytotoxicity

As shown in Figure 4.5.A, NP1-siRNA complexes at 6 uM NP1concentration and 100 nM siRNA achieved 85% and NP1 alone had a slight drop to 73% due to to relatively higher positive surface charge. Complexing Np1 with siRNA reduced the surface positive charge by neutralizing with negatively charged siRNA.

WST-1 assay was used to determine the viability of the HCT 116 spheroids 48 hours post treatment. As shown in Figure 4.5.B, NP1 complexed with Bcl-2 and VEGF siRNAs did not cause cytotoxicity, achieved >95% viability at all treatments. This phenomenon of gene and chemotherapy therapy resistance in tumor *in vivo* has been reported[81,82]. Suggesting that 3D spheroids generated in hanging drop plate reassemble the tumor microenvironment *in vivo*.

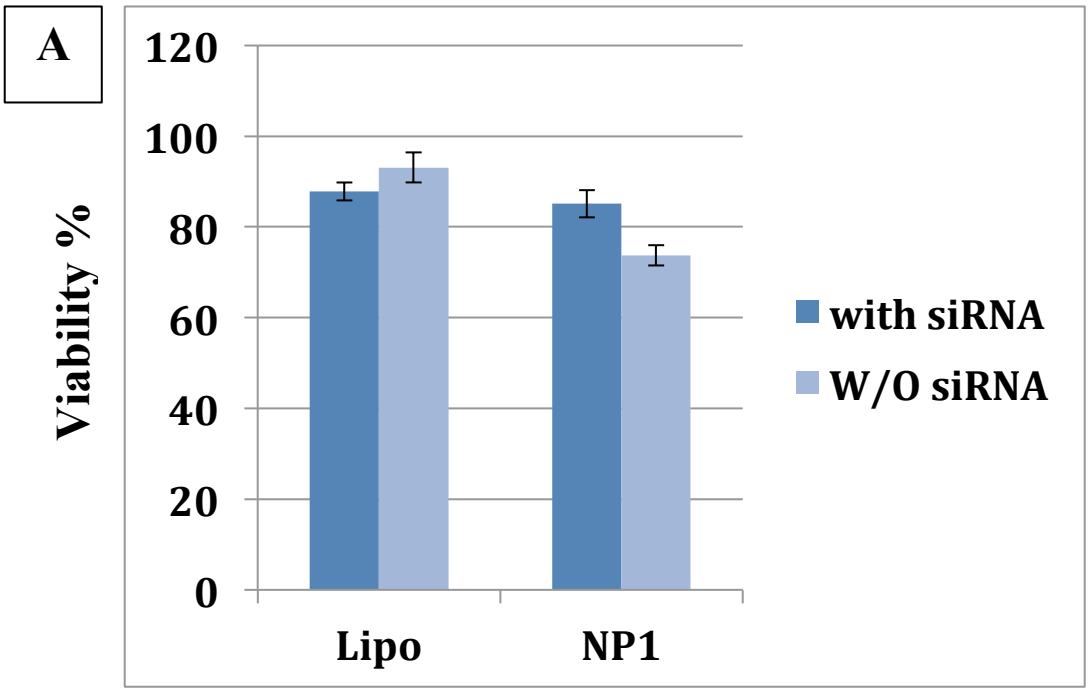

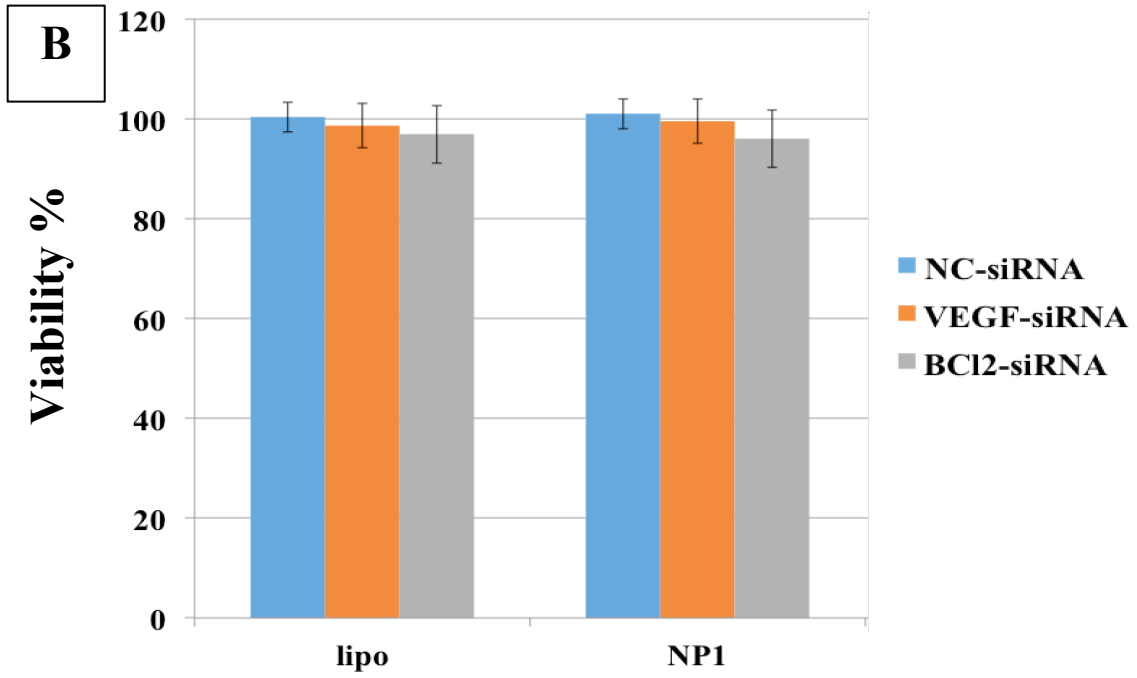

Figure 4.5. Cell viability results of HCT 116 cells treated with different complexes of NP1 and Lipo siRNAs. (A) 2D cell monolayer viability 24 hours post transfection with NP1 peptide alone or in complex with siRNA at 60/1 molar ratio. (B) 3D spheroid viability 48 hours post transfection with NP1 complexed with three siRNAs (VEGF, Bcl-2 and scrambled siRNA used as a control). (NC=negative control, Lipo=Lipofectamine 2000). Results are expressed as mean ± standard deviation (n=3).

4.4 *In Vitro* Transfection Efficiency

To confirm the delivered siRNA performed its function, RT-PCR measurement of Bcl-2 and VEGFR mRNA level in the HCT 116 cells in both 2D and 3D cell culture methods, was performed. Cyclophilin is a housekeeping gene was used as a control, where its mRNA level remained relatively stable during the transfection experiments. As shown in Figure 4.6.B, the gene silencing efficiency induced by NP1-Bcl-2-siRNA complex at 60/1 with siRNA concentration of 100 nM 85%. The NP1-VEGF-siRNA complex at the similar transfection condition induced 72% gene knockdown efficiency. The silencing efficiency of NP1 was similar to that of a benchmark, Lipofactamine 2000 (Lipo), which is the most commonly utilized and efficient transfection reagent to introduce siRNA into cells, inducing 82% and 71% gene silencing for Bcl-2 and VEGF siRNAs, respectively. This result indicated that NP1 could efficiently protect and deliver siRNA to cells and induced the specific gene silencing. The high efficiency, possibly due to the rapid and efficient internalization of NP1 complexes to the cells and successful release of siRNA from endosome, to react with RISC in the cytoplasm and subsequently induce the knockdown to the targeted genes.

In 3D spheroids, cells were collected 96 hours post transfection with NP1-siRNA complexes for RT-PCR analysis. Longer time was performed due to the slower penetration in spheroids compare to 2D cell monolayer. However, the uptake of NP1 was reduced compared to 2D cell monolayer, NP1 achieved higher silencing efficiency than Lipo2000. Figure 4.6.C, the gene silencing efficiency induced by NP1-Bcl-2-siRNA and NP1-VEGF-siRNA complexes 53% and 51% respectively. The NP1-VEGF-siRNA complex at the similar transfection condition induced 72% gene knockdown efficiency.

Lipo2000 induced 39% and 35% gene silencing for Bcl-2 and VEGF siRNAs, respectively. The relatively large particle size of Lipofectamine 2000-siRNA complexes around (340 nm) compare to NP1 (<100 nm), possibly limited the cellular uptake of siRNA within the internal layers of the multicellular tumor spheroids, thus leading to a relatively lower gene silencing efficiency. Additionally, as discussed before, positively charged nanoparticles could preferentially retained by negative surface charges on ECM and taken up by proliferating cells in the outer layer of the spheroids which mean that NP1 is highly targeting the proliferating cells that produce more proteins compare to the dormant cells in internal layers of the spheroids. The results were further confirmed at protein level by Western blot to measure the expression of Bcl-2 protein 3D tumor spheroids post transfection. The results shown in Figure 4.6.A, demonstrates that the expression of Bcl-2 protein was significantly inhibited in spheroids treated with NP1-Bcl-2-siRNA compare to non-treated cells.

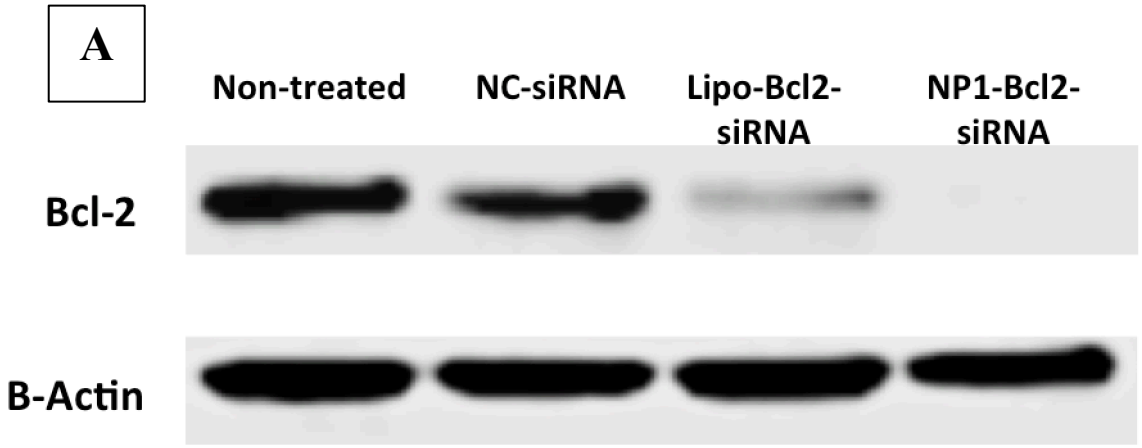

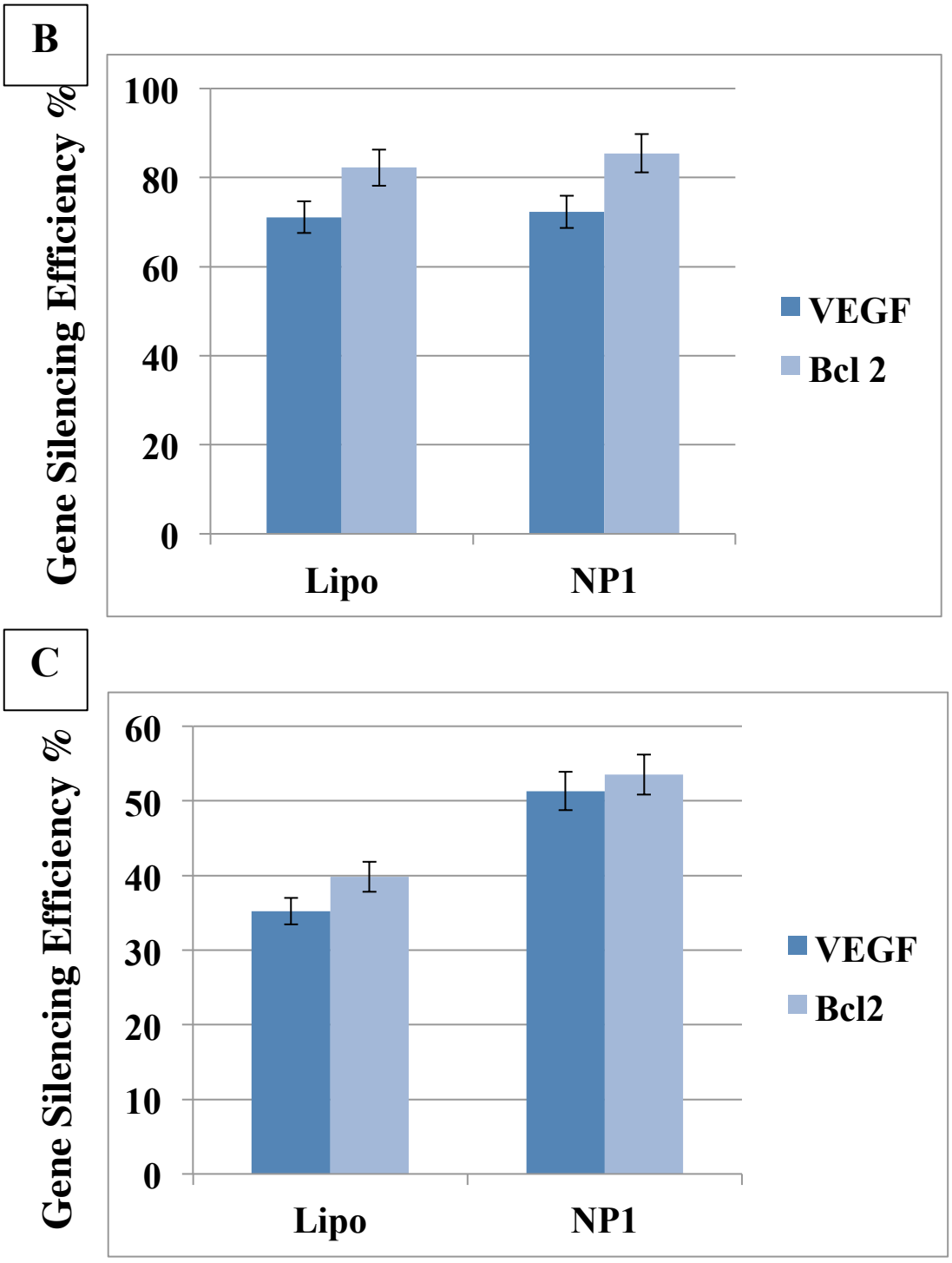

Figure 4.6. Gene silencing efficiency *in vitro*. (A) Silencing efficiency at protein level. Total proteins were extracted from HCT 116 3D spheroids. Bcl-2 protein expression was detected by western blot. House keeping protein B-actin was used as control.

(B) Silencing of VEGF and Bcl-2 genes in 2D HCT 116 cells was evaluated by quantitative real time polymerase chain reaction (qRT-PCR). NP1concentration was 6 uM and siRNA100 nM. Total RNA was extracted 48 hours post transfection and gene knockdown efficiency was determined. (C) Silencing efficiency of VEGF and Bcl-2 genes in 3D HCT 116 spheroids 96 hours post transfection. All the data were normalized to house keeping gene cyclophilin. Lipofectamine 2000 was the positive control. Results are expressed as mean ± standard deviation (n=3).

4.5 Induced Apoptosis

Spheroids and 2D monolayer cells treated by NP1-siRNA complexes where tested for induced apoptosis by Apoptosis Kit with Annexin V FITC and PI (flow cytometry). All siRNA complexes induce higher apoptosis compare to the non-treated cells (Figure 4.7). The highest apoptosis was induced in cells treated by Bcl-2 in both cell culture methods and was significantly higher than induced apoptosis in cells treated by VEGF siRNA. Bcl-2 is anti-apoptotic marker over expressed in many human tumors and considered as an important oncogene. Suppression or silencing of Bcl-2 proves to induce apoptosis and reduce the tumor growth[32]. Furthermore, the cells undergoing apoptosis in 2D cell monolayer are higher than 3D spheroids post transfection with Bcl-2 and VEGF siRNA. 3D MCSs exhibit decreased sensitivity to chemotherapeutic drugs or gene therapies, the resistance may be caused by hypoxia in MCSs. Hypoxia associated with an increased cell population in G0 and early G1 phase and/or down regulation of pro-apoptotic molecules such as caspase-3, therefore more resistant to apoptosis compare to 2D cell monolayer[83]. Concluding that 3D culture systems are better in simulating the *in*

vivo tumor microenvironment compare to 2D cells grown on plastic surfaces that are unable to precisely simulate tumor conditions *in vivo*[84–87].

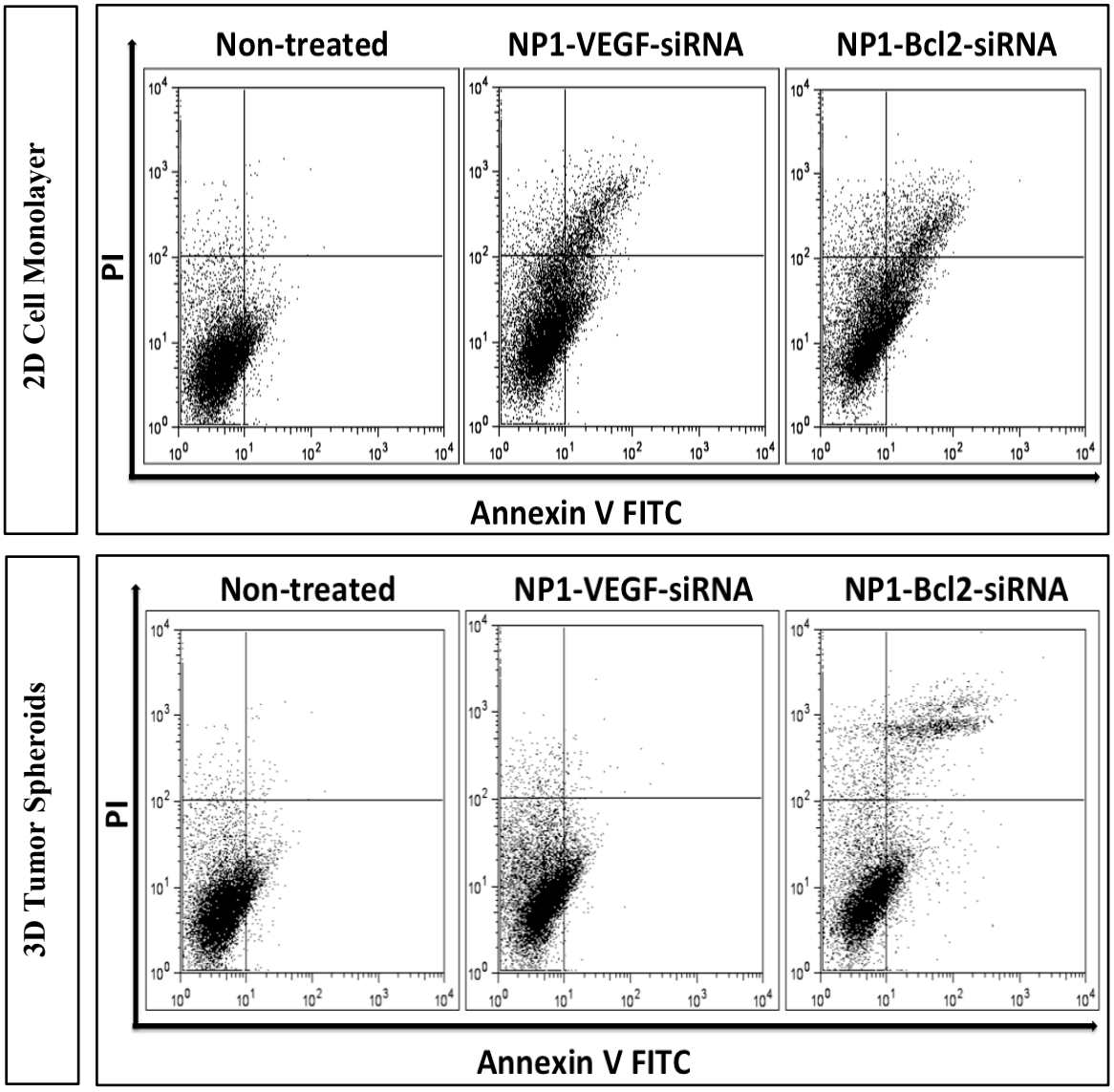

Figure 4.7. Induced apoptosis by FACS analysis, using Apoptosis Kit with Annexin V FITC and PI. Cells positive for Annexin V are in early apoptosis and cells positive for both PI and Annexin V are in late apoptosis (n=3).

4.6 Histological Evaluation

4.6.1 Routine H&E Staining

In histopathology, the term “routine staining” refers to the hematoxylin and eosin stain (H&E) which used with all tissue specimens, H&E staining play a critical role in tissue-based diagnosis, allow to visualize the tissue morphology (structure) and cell types. Hematoxylin is a basic dye with a purplish blue color and generally stains acidic, or basophilic, structure including the cell nucleous and organelles that contain RNA. Whereas, eosin is an acidic dye with reddish or pink color and stains basic, or acidophilic, structures including the cytoplasm and extracellular fibers. General observations from routine H&E staining, stained sections of spheroids show large cohesive cells with apparent epithelial phenotype, pronounced cell contours, abundant eosinophilic cytoplasm and large atypical nuclei with occasional prominent nucleoli (Figure 4). These observations are clear evident that 3D spheroids generated in hanging drop resample the tumour microenvironment *in vivo*. Nucleolus size represents series of metabolic changes that characterize cancer cells. The enlargement of nucleolar size is an indicator of entry into the cell cycle, which normally associated with up-regulation of the nucleolar function. A major feature of cancer cells is high uncontrollable cell growth rate and disruption of the tumour suppressor retinoblastoma Rb and p53 pathways, leading for greater aggressiveness. Therefore, prominent nucleolus is a clear predictive and prognostic parameter of malignant tumour. Furthermore, cells demonstrate high degree of pleiomorphism, hyperchromasia and atypical mitotic figures such as metaphase and anaphase as shown in (Figure 4.8.E). In Figure 4.8.C, clear presence of apoptotic bodies predominantly located in the central regions of the spheroids, supporting previous results

of presence of necrotic core. Minimal areas with amorphous material possibly necrotic or disorganized matrix material are also present (Figure 4.8.D).

4.6.2 Immunohistochemichal Analysis for Proliferation Marker Ki-67

Ki-67 proliferation marker was used to investigate the internal structure of the spheroids immunohistochemicaly. Ki-67 is an immunohistochemical proliferation marker expressed in all proliferating cells[88,89]. For spheroids cultured for 7 days and stained with Ki-67 marker, proliferation (immunopositivity) is more pronounced in the periphery of the spheroids, indicating that the cells are viable and actively dividing. Central zones show markedly reduced proliferation, indicative of slowed down cellular turnover or increased number of degenerating and dying cells as shown in (Figure 4.9.C). The reason more proliferating cells at the periphery or the outer layers is du to direct contact of the cells with the culturing medium providing essential nutrient and oxygen for normal cell growth, wile the cells in the internal layers receive less as a result of gradient diffusion of oxygen and nutrient. Similar pattern observed as in Figure 4.3, and therefore mimic the *in vivo* microenvironment of tumor. Figure 4.9.D, spheroid collected at day 7, 3 days post treatment with NP1 peptide without siRNA. Normal distribution of Ki-67 was observed; more pronounced in the periphery and less in the center indicating that NP1 is relatively safe carrier and did not affect the cell growth kinetics through the spheroid. Interestingly, spheroids treated with NP1-HIF-siRNA, the proliferation (immunopositivity) is more uniform, periphery is not significantly more mitotically active than the central and paracentral regions, possibly indicating similar number of viable and regenerating cells in the periphery and the central regions of the spheroids (Figure 4.9.E-F). This indicated that NP1 deliver HIF-siRNA successfully to the spheroids, where HIF is hypoxia inducible

factor. Higher expression of ki-67 through the spheroid and uniform distribution even in the central region is a clear indicator of reduction of hypoxia. Ki67 is a non-histone nuclear protein, tightly linked to the cell cycle and present during all active phases of the cell cycle: during mid G1, increasing through S and G_2 and peaking in the M phase, but absent in resting dormant cells in G_0 and early G_1[90,91]. Furthermore, hypoxia has been reported to cause cancer cell dormancy and arresting cell cycle in the G0 or early G1 phase [83,92].Therfore, HIF-siRNA reduce the hypoxia which cause the cancer cells more resistant for chemo or gene therapy and the cells were entering different stages of cell cycle which cause cell death later as the cells need more nutrient and oxygen for normal cell growth due to gradient diffusion as discussed before.

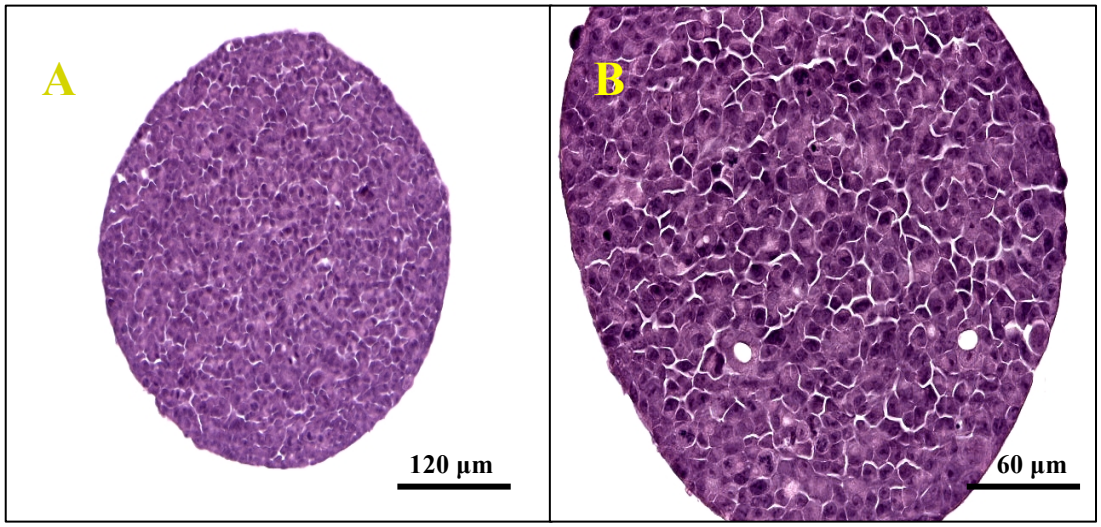

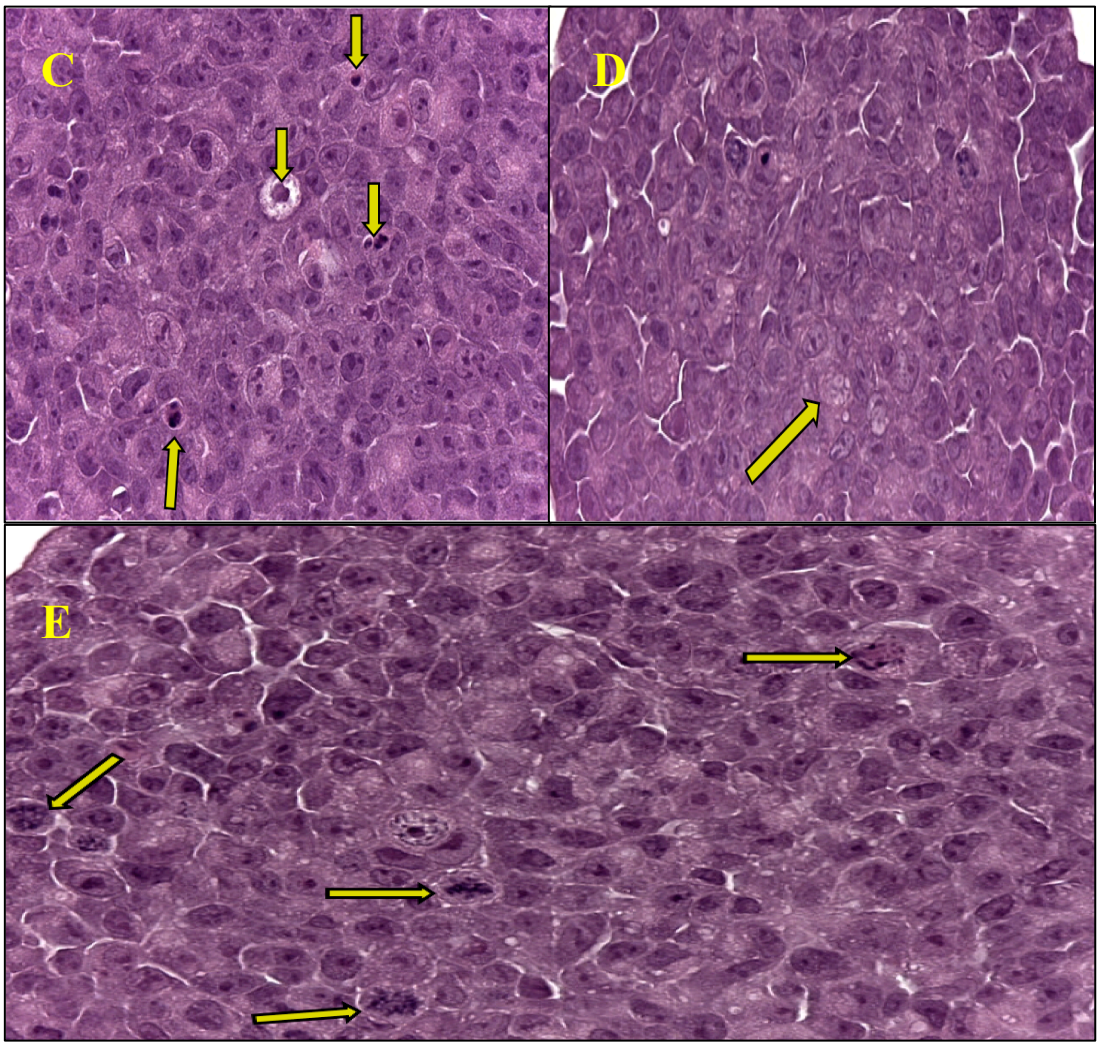

Figure 4.8. Routine H&E staining of HCT 116 spheroids. (A&B) Represent the overall morphology of spherical micro-tissues, darker purplish blue staining is the nucleus and brighter are the cytoplasm and ECM. (C) Cellular degeneration, fragmentation and apoptotic bodies (arrow). (D) Amorphous material possibly disorganized matrix or degenerating cellular debris (arrow). (E) Atypical mitotic figures and irregular chromatin pattern (arrow).

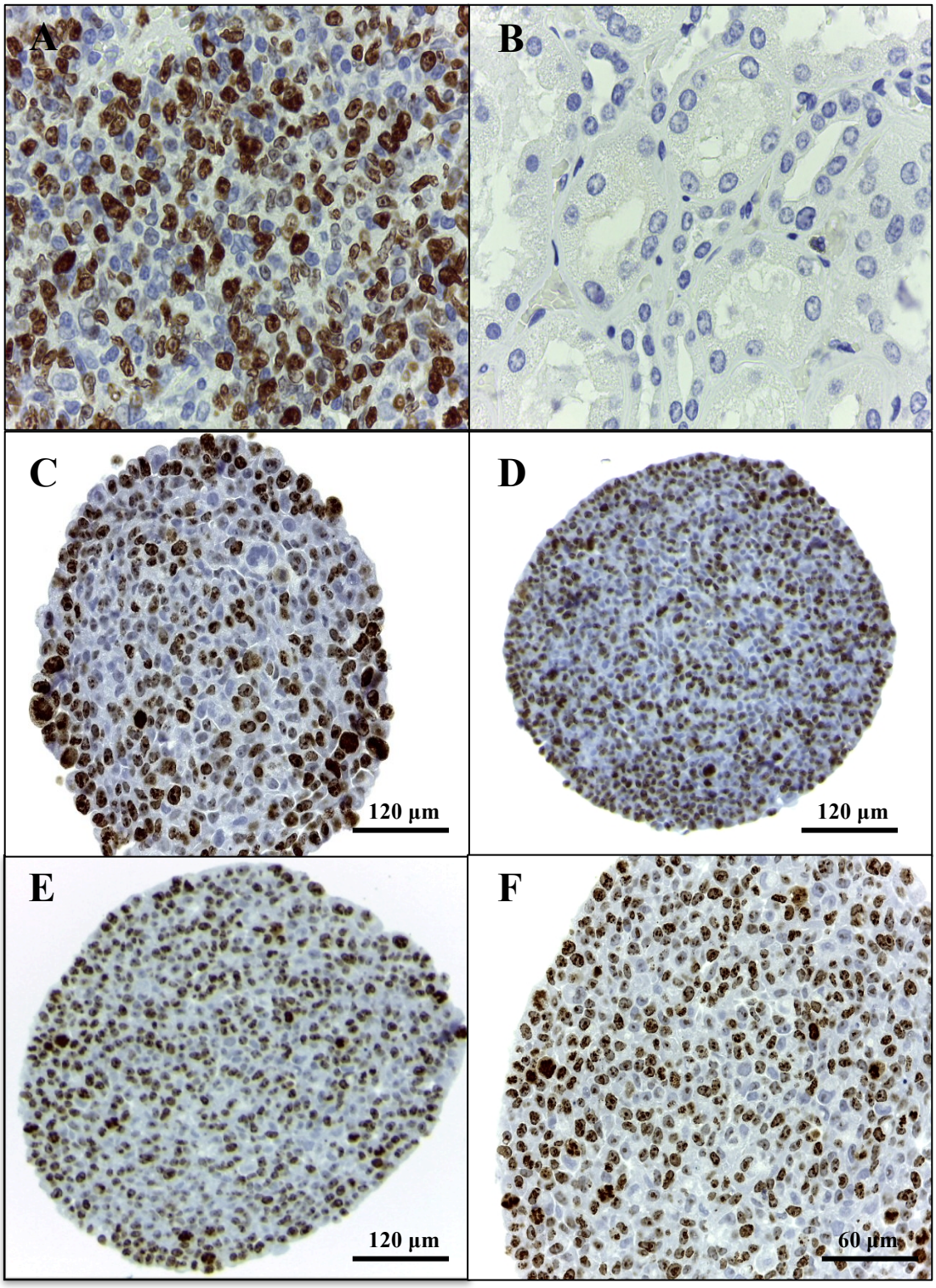

Figure 4.9. Immunohistochemichal analysis for proliferation marker Ki-67 in 3D HCT 116 spheroids. (A) Positive control – immunopositive cells (staining in brown) in a

germinal center of a lymph node. (B) Negative control- no staining (no primary antibody added). (C) Spheroids cultured for 7 days and stained with Ki-67 marker, proliferation (immunopositivity cells stained brown) is more pronounced in the periphery of the spheroids. (D) Spheroids transfected with NP1 free peptide and collected 72 hours post transfection. (E-F) spheroids transfected with NP1-HIF-siRNA and collected 72 hours post transfection.

Chapter 5
Conclusions and Recommendations

Cell penetrating peptides delivery systems have recently emerged as a promising candidate to transport the therapeutic genes into targeted cells. Most nanoparticles used for drug or gene therapy have been extensively evaluated in 2D cell monolayer, which overestimates the efficacies of chemotherapeutic drugs. Our studies suggest that 3D cultured cells forming compact MCTS closely mimic the features of tumors *in vivo* in term of simulating important tumor characteristics including hypoxia, formation of proliferating rim and necrotic core, formation of ECM, anti-apoptotic features and their resulting therapy resistance. Morphological characterization of 3D spheroids generated in hanging drop plats, clearly indicate that HCT 116 cells were able to form compact spheroids within 3 days and start to form three distinct layers of proliferating, dormant and necrotic cells as utilized by confocal laser scanning microscopy. Further more, SEM images proved the ability of 3D spheroids to form ECM with time and enhance the cellular interaction. General observations from routine H&E staining, such as large cohesive cells with apparent epithelial phenotype, and large atypical nuclei with occasional prominent nucleoli also support that 3D spheroids resample *in vivo* tumors.

NP1 demonstrated high gene knockdown efficiency, both in 2D and 3D cell culture in colon caner cell line HCT 116. The uptake of NP1 complexes in 2D monolayer cells was significantly higher compared to the commercial transfection reagent, Lipofectamine 2000, but was slowed down in 3D spheroids. Confocal images and FACS results showed the ability of NP1 complexes to penetrate through the spheroids over the time. Slight

cytotoxicity was observed in 2D cell monolayer but very minimal in multicellular tumor spheroids (<5%). NP1-Bcl-2-siRNA complexes exhibited significant inhibition of Bcl-2 protein compare to non-treated cells in western blot results. Induced apoptosis in 2D and 3D cell culture demonstrate the efficiency of NP1 in delivering siRNA to targeted cells and cause higher apoptosis compare to non-treated cells. In 3D spheroids apoptosis resistance was observed compared to 2D cells. NP1 is a highly promising siRNA delivery vector in 2D cell monolayer and 3D tumor spheroids.

Based on the findings in this research, the following recommendations for future studies are proposed:

1) Developing more complex 3D tumor by implying some features of *in vivo* tumor microenvironment including:

- Rigidity of ECM by impeding the spheroids in hydrogels.
- Co-culturing the cancer cells with normal fibroblast cells that normally present *in vivo* and play critical role in tumor growth and survival.

2) Developing *in vitro* tumor tissues by bio-printing that will reduce the limitations of regular 3D culture methods and provide more platform model for early drug screening.

3) Further modification of NP1 to enhance the internalization in 3D spheroids and enhance the compatibility possibly by PEGylation.

References

1. Ambesajir, A., Kaushik, A., Kaushik, J. J. & Petros, S. T. RNA interference: A futuristic tool and its therapeutic applications. *Saudi J Biol Sci* **19,** 395–403 (2012).
2. Elbashir, S. M., Lendeckel, W. & Tuschl, T. RNA interference is mediated by 21- and 22-nucleotide RNAs. *Genes Dev.* **15,** 188–200 (2001).
3. Zou, G.-M. & Yoder, M. C. Application of RNA interference to study stem cell function: current status and future perspectives. *Biology of the Cell* **97,** 211–219 (2005).
4. Tang, G. siRNA and miRNA: an insight into RISCs. *Trends Biochem. Sci.* **30,** 106–114 (2005).
5. Matranga, C., Tomari, Y., Shin, C., Bartel, D. P. & Zamore, P. D. Passenger-strand cleavage facilitates assembly of siRNA into Ago2-containing RNAi enzyme complexes. *Cell* **123,** 607–620 (2005).
6. Gregory, R. I., Chendrimada, T. P., Cooch, N. & Shiekhattar, R. Human RISC couples microRNA biogenesis and posttranscriptional gene silencing. *Cell* **123,** 631–640 (2005).
7. Chendrimada, T. P. *et al.* TRBP recruits the Dicer complex to Ago2 for microRNA processing and gene silencing. *Nature* **436,** 740–744 (2005).
8. Wang, J., Lu, Z., Wientjes, M. G. & Au, J. L.-S. Delivery of siRNA Therapeutics: Barriers and Carriers. *AAPS J* **12,** 492–503 (2010).
9. Shim, M. S. & Kwon, Y. J. Efficient and targeted delivery of siRNA in vivo. *FEBS J.* **277,** 4814–4827 (2010).

10. Tomar, R. S., Matta, H. & Chaudhary, P. M. Use of adeno-associated viral vector for delivery of small interfering RNA. *Oncogene* **22,** 5712–5715 (2003).
11. Tseng, Y.-C., Mozumdar, S. & Huang, L. Lipid-based systemic delivery of siRNA. *Adv Drug Deliv Rev* **61,** 721–731 (2009).
12. Gary, D. J., Puri, N. & Won, Y.-Y. Polymer-based siRNA delivery: Perspectives on the fundamental and phenomenological distinctions from polymer-based DNA delivery. *Journal of Controlled Release* **121,** 64–73 (2007).
13. Biswas, S. & Torchilin, V. P. Dendrimers for siRNA Delivery. *Pharmaceuticals (Basel)* **6,** 161–183 (2013).
14. Crombez, L. & Divita, G. A non-covalent peptide-based strategy for siRNA delivery. *Methods Mol. Biol.* **683,** 349–360 (2011).
15. Draz, M. S. *et al.* Nanoparticle-Mediated Systemic Delivery of siRNA for Treatment of Cancers and Viral Infections. *Theranostics* **4,** 872–892 (2014).
16. Chu, D. *et al.* Rational modification of oligoarginine for highly efficient siRNA delivery: structure–activity relationship and mechanism of intracellular trafficking of siRNA. *Nanomedicine: Nanotechnology, Biology and Medicine* **11,** 435–446 (2015).
17. Haycock, J. W. 3D cell culture: a review of current approaches and techniques. *Methods Mol. Biol.* **695,** 1–15 (2011).
18. Mehta, G., Hsiao, A. Y., Ingram, M., Luker, G. D. & Takayama, S. Opportunities and challenges for use of tumor spheroids as models to test drug delivery and efficacy. *Journal of Controlled Release* **164,** 192–204 (2012).
19. Whitehead, K. A., Langer, R. & Anderson, D. G. Knocking down barriers: advances in siRNA delivery. *Nat Rev Drug Discov* **8,** 129–138 (2009).

20. Czech, M. P., Aouadi, M. & Tesz, G. J. RNAi-based therapeutic strategies for metabolic disease. *Nat Rev Endocrinol* **7,** 473–484 (2011).
21. Manfredsson, F. P., Lewin, A. S. & Mandel, R. J. RNA knockdown as a potential therapeutic strategy in Parkinson's disease. *Gene Ther.* **13,** 517–524 (2006).
22. Jacque, J.-M., Triques, K. & Stevenson, M. Modulation of HIV-1 replication by RNA interference. *Nature* **418,** 435–438 (2002).
23. Klein, C. *et al.* Inhibition of hepatitis B virus replication in vivo by nucleoside analogues and siRNA. *Gastroenterology* **125,** 9–18 (2003).
24. Hibbitt, O. *et al.* RNAi-mediated knockdown of HMG CoA reductase enhances gene expression from physiologically regulated low-density lipoprotein receptor therapeutic vectors in vivo. *Gene Ther.* **19,** 463–467 (2012).
25. Bumcrot, D., Manoharan, M., Koteliansky, V. & Sah, D. W. Y. RNAi therapeutics: a potential new class of pharmaceutical drugs. *Nat Chem Biol* **2,** 711–719 (2006).
26. Deng, Y. *et al.* Therapeutic potentials of gene silencing by RNA interference: Principles, challenges, and new strategies. *Gene* **538,** 217–227 (2014).
27. McLeod, H. L. Cancer pharmacogenomics: early promise, but concerted effort needed. *Science* **339,** 1563–1566 (2013).
28. Suvà, M. L., Riggi, N. & Bernstein, B. E. Epigenetic reprogramming in cancer. *Science* **339,** 1567–1570 (2013).
29. Bora, R. S., Gupta, D., Mukkur, T. K. S. & Saini, K. S. RNA interference therapeutics for cancer: challenges and opportunities (review). *Mol Med Rep* **6,** 9–15 (2012).

30. Ramachandran, P. V. & Ignacimuthu, S. RNA interference as a plausible anticancer therapeutic tool. *Asian Pac. J. Cancer Prev.* **13,** 2445–2452 (2012).

31. Huang, P.-I. *et al.* Non-viral delivery of RNA interference targeting cancer cells in cancer gene therapy. *Curr Gene Ther* **12,** 275–284 (2012).

32. Tomek, M., Akiyama, T. & Dass, C. R. Role of Bcl-2 in tumour cell survival and implications for pharmacotherapy. *J. Pharm. Pharmacol.* **64,** 1695–1702 (2012).

33. Doan, C. C., Le, L. T., Hoang, S. N., Do, S. M. & Le, D. V. Simultaneous silencing of VEGF and KSP by siRNA cocktail inhibits proliferation and induces apoptosis of hepatocellular carcinoma Hep3B cells. *Biol Res* **47,** (2014).

34. Fakih, M. The evolving role of VEGF-targeted therapies in the treatment of metastatic colorectal cancer. *Expert Rev Anticancer Ther* **13,** 427–438 (2013).

35. Michaylira, C. Z. & Nakagawa, H. Hypoxic microenvironment as a cradle for melanoma development and progression. *Cancer Biol. Ther.* **5,** 476–479 (2006).

36. Koh, M. Y., Spivak-Kroizman, T. R. & Powis, G. HIF-1alpha and cancer therapy. *Recent Results Cancer Res.* **180,** 15–34 (2010).

37. Liu, X.-Q., Xiong, M.-H., Shu, X.-T., Tang, R.-Z. & Wang, J. Therapeutic delivery of siRNA silencing HIF-1 alpha with micellar nanoparticles inhibits hypoxic tumor growth. *Mol. Pharm.* **9,** 2863–2874 (2012).

38. Tan, F. L. & Yin, J. Q. RNAi, a new therapeutic strategy against viral infection. *Cell Res* **14,** 460–466 (2004).

39. Bobbin, M. L., Burnett, J. C. & Rossi, J. J. RNA interference approaches for treatment of HIV-1 infection. *Genome Med* **7,** (2015).

40. Chen, Y. & Mahato, R. I. siRNA Pool Targeting Different Sites of Human Hepatitis B Surface Antigen Efficiently Inhibits HBV Infection. *J Drug Target* **16,** 140–148 (2008).

41. Wieland, S. F. & Chisari, F. V. Stealth and Cunning: Hepatitis B and Hepatitis C Viruses. *J. Virol.* **79,** 9369–9380 (2005).

42. McCaffrey, A. P. *et al.* Inhibition of hepatitis B virus in mice by RNA interference. *Nat. Biotechnol.* **21,** 639–644 (2003).

43. Sheikh, S. *et al.* Neurodegenerative Diseases: Multifactorial Conformational Diseases and Their Therapeutic Interventions, Neurodegenerative Diseases: Multifactorial Conformational Diseases and Their Therapeutic Interventions. *Journal of Neurodegenerative Diseases, Journal of Neurodegenerative Diseases* **2013, 2013,** e563481 (2012).

44. Higuchi, H., Yamashita, T., Yoshikawa, H. & Tohyama, M. Functional inhibition of the p75 receptor using a small interfering RNA. *Biochemical and Biophysical Research Communications* **301,** 804–809 (2003).

45. Colussi, P. A. *et al.* Debcl, a proapoptotic Bcl-2 homologue, is a component of the Drosophila melanogaster cell death machinery. *J. Cell Biol.* **148,** 703–714 (2000).

46. Quinn, L. M. *et al.* An essential role for the caspase dronc in developmentally programmed cell death in Drosophila. *J. Biol. Chem.* **275,** 40416–40424 (2000).

47. Xu, C. & Wang, J. Delivery systems for siRNA drug development in cancer therapy. *Asian Journal of Pharmaceutical Sciences* **10,** 1–12 (2015).

48. Burchard, J. *et al.* MicroRNA-like off-target transcript regulation by siRNAs is species specific. *RNA* **15,** 308–315 (2009).

49. Robbins, M., Judge, A. & MacLachlan, I. siRNA and innate immunity. *Oligonucleotides* **19,** 89–102 (2009).

50. Karikó, K., Bhuyan, P., Capodici, J. & Weissman, D. Small interfering RNAs mediate sequence-independent gene suppression and induce immune activation by signaling through toll-like receptor 3. *J. Immunol.* **172,** 6545–6549 (2004).

51. Marques, J. T. & Williams, B. R. G. Activation of the mammalian immune system by siRNAs. *Nat Biotech* **23,** 1399–1405 (2005).

52. Wu, G. Y. & Wu, C. H. Receptor-mediated in vitro gene transformation by a soluble DNA carrier system. *J. Biol. Chem.* **262,** 4429–4432 (1987).

53. Nayerossadat, N., Maedeh, T. & Ali, P. A. Viral and nonviral delivery systems for gene delivery. *Adv Biomed Res* **1,** (2012).

54. Khan, A. *et al.* Sustained polymeric delivery of gene silencing antisense ODNs, siRNA, DNAzymes and ribozymes: in vitro and in vivo studies. *J Drug Target* **12,** 393–404 (2004).

55. Goyal, P. *et al.* Liposomal drug delivery systems--clinical applications. *Acta Pharm* **55,** 1–25 (2005).

56. Hong, C. A. & Nam, Y. S. Functional Nanostructures for Effective Delivery of Small Interfering RNA Therapeutics. *Theranostics* **4,** 1211–1232 (2014).

57. Xue, H. Y., Guo, P., Wen, W.-C. & Wong, H. L. Lipid-Based Nanocarriers for RNA Delivery. *Curr Pharm Des* **21,** 3140–3147 (2015).

58. Pathak, K., Keshri, L. & Shah, M. Lipid nanocarriers: influence of lipids on product development and pharmacokinetics. *Crit Rev Ther Drug Carrier Syst* **28,** 357–393 (2011).

59. Mallick, S. & Choi, J. S. Liposomes: versatile and biocompatible nanovesicles for efficient biomolecules delivery. *J Nanosci Nanotechnol* **14,** 755–765 (2014).

60. Li, W. & Szoka, F. C. Lipid-based nanoparticles for nucleic acid delivery. *Pharm. Res.* **24,** 438–449 (2007).

61. Zhang, C. *et al.* siRNA-containing liposomes modified with polyarginine effectively silence the targeted gene. *Journal of Controlled Release* **112,** 229–239 (2006).

62. Ren, T., Song, Y. K., Zhang, G. & Liu, D. Structural basis of DOTMA for its high intravenous transfection activity in mouse. *Gene Ther.* **7,** 764–768 (2000).

63. Prasad, T. K., Gopal, V. & Rao, N. M. Cationic lipids and cationic ligands induce DNA helix denaturation: detection of single stranded regions by KMnO4 probing. *FEBS Letters* **552,** 199–206 (2003).

64. Jeong, J. H., Park, T. G. & Kim, S. H. Self-Assembled and Nanostructured siRNA Delivery Systems. *Pharm Res* **28,** 2072–2085 (2011).

65. Khalil, I. A., Kogure, K., Futaki, S. & Harashima, H. Octaarginine-modified liposomes: enhanced cellular uptake and controlled intracellular trafficking. *Int J Pharm* **354,** 39–48 (2008).

66. Farkhani, S. M. *et al.* Cell penetrating peptides: Efficient vectors for delivery of nanoparticles, nanocarriers, therapeutic and diagnostic molecules. *Peptides* **57,** 78–94 (2014).

67. Green, M., Ishino, M. & Loewenstein, P. M. Mutational analysis of HIV-1 Tat minimal domain peptides: Identification of trans-dominant mutants that suppress HIV-LTR-driven gene expression. *Cell* **58,** 215–223 (1989).

68. Futaki, S. *et al.* Arginine-rich peptides. An abundant source of membrane-permeable peptides having potential as carriers for intracellular protein delivery. *J. Biol. Chem.* **276,** 5836–5840 (2001).

69. Milletti, F. Cell-penetrating peptides: classes, origin, and current landscape. *Drug Discovery Today* **17,** 850–860 (2012).

70. Bolhassani, A. Potential efficacy of cell-penetrating peptides for nucleic acid and drug delivery in cancer. *Biochim. Biophys. Acta* **1816,** 232–246 (2011).

71. van Asbeck, A. H. *et al.* Molecular Parameters of siRNA–Cell Penetrating Peptide Nanocomplexes for Efficient Cellular Delivery. *ACS Nano* **7,** 3797–3807 (2013).

72. Hynes, R. O. The Extracellular Matrix: Not Just Pretty Fibrils. *Science* **326,** 1216–1219 (2009).

73. Järveläinen, H., Sainio, A., Koulu, M., Wight, T. N. & Penttinen, R. Extracellular matrix molecules: potential targets in pharmacotherapy. *Pharmacol. Rev.* **61,** 198–223 (2009).

74. Godugu, C. *et al.* AlgiMatrix^{TM} Based 3D Cell Culture System as an In-Vitro Tumor Model for Anticancer Studies. *PLoS One* **8,** (2013).

75. Santini, M. T. & Rainaldi, G. Three-dimensional spheroid model in tumor biology. *Pathobiology* **67,** 148–157 (1999).

76. Santini, M. T., Rainaldi, G. & Indovina, P. L. Apoptosis, cell adhesion and the extracellular matrix in the three-dimensional growth of multicellular tumor spheroids. *Critical Reviews in Oncology/Hematology* **36,** 75–87 (2000).

77. Fuchs, S. M. & Raines, R. T. Internalization of Cationic Peptides: The road less (or more?) traveled. *Cell Mol Life Sci* **63,** 1819–1822 (2006).

78. Minchinton, A. I. & Tannock, I. F. Drug penetration in solid tumours. *Nat. Rev. Cancer* **6,** 583–592 (2006).

79. Ma, H. *et al.* Multicellular tumor spheroids as an in vivo-like tumor model for three-dimensional imaging of chemotherapeutic and nano material cellular penetration. *Mol Imaging* **11,** 487–498 (2012).

80. Kim, B. *et al.* Tuning payload delivery in tumour cylindroids using gold nanoparticles. *Nat Nano* **5,** 465–472 (2010).

81. Zaboikin, M., Srinivasakumar, N. & Schuening, F. Gene therapy with drug resistance genes. *Cancer Gene Ther.* **13,** 335–345 (2006).

82. Roth, J. A. & Cristiano, R. J. Gene Therapy for Cancer: What Have We Done and Where Are We Going? *JNCI J Natl Cancer Inst* **89,** 21–39 (1997).

83. Imamura, Y. *et al.* Comparison of 2D- and 3D-culture models as drug-testing platforms in breast cancer. *Oncology Reports* (2015). doi:10.3892/or.2015.3767

84. Hirschhaeuser, F. *et al.* Multicellular tumor spheroids: an underestimated tool is catching up again. *J. Biotechnol.* **148,** 3–15 (2010).

85. Rimann, M. & Graf-Hausner, U. Synthetic 3D multicellular systems for drug development. *Current Opinion in Biotechnology* **23,** 803–809 (2012).

86. Breslin, S. & O'Driscoll, L. Three-dimensional cell culture: the missing link in drug discovery. *Drug Discovery Today* **18,** 240–249 (2013).

87. Lovitt, C. J., Shelper, T. B. & Avery, V. M. Advanced Cell Culture Techniques for Cancer Drug Discovery. *Biology* **3,** 345–367 (2014).

88. Jalava, P. *et al.* Ki67 immunohistochemistry: a valuable marker in prognostication but with a risk of misclassification: proliferation subgroups formed based on Ki67

immunoreactivity and standardized mitotic index. *Histopathology* **48,** 674–682 (2006).

89. Kontzoglou, K. *et al.* Correlation between Ki67 and breast cancer prognosis. *Oncology* **84,** 219–225 (2013).
90. Tan, P.-H. *et al.* Immunohistochemical detection of Ki67 in breast cancer correlates with transcriptional regulation of genes related to apoptosis and cell death. *Mod Pathol* **18,** 374–381 (2004).
91. Gerdes, J. *et al.* Cell cycle analysis of a cell proliferation-associated human nuclear antigen defined by the monoclonal antibody Ki-67. *J. Immunol.* **133,** 1710–1715 (1984).
92. Sullivan, R. & Graham, C. H. Hypoxia prevents etoposide-induced DNA damage in cancer cells through a mechanism involving hypoxia-inducible factor 1. *Mol. Cancer Ther.* **8,** 1702–1713 (2009).